The Thesis Committee for Corey John Van Dyk
Certifies that this is the approved version of the following thesis:

Validation of a reduced-complexity numerical model for resolving deltaic dynamics: internal consistency and morphodynamics

APPROVED BY
SUPERVISING COMMITTEE:

Supervisor:

Paola Passalacqua

David Mohrig

Validation of a reduced-complexity numerical model for resolving deltaic dynamics: internal consistency and morphodynamics

by

Corey John Van Dyk, BSE

Thesis

Presented to the Faculty of the Graduate School of

The University of Texas at Austin

in Partial Fulfillment

of the Requirements

for the Degree of

Master of Science in Engineering

The University of Texas at Austin

May 2015

Acknowledgements

The work presented herein was made possible by the National Science Foundation Award Numbers CAREER/EAR – 1350336 and FESD/OCE – 1135427.

I would first like to thank those at the University of Texas at Austin who played a role in my learning and work. First of all, I am very grateful to my advisor, Dr. Paola Passalacqua, for guiding my research, directing my curiosity, and displaying patience and enthusiasm with regards to my scientific journey. I am thankful also for Dr. David Mohrig and his constructive direction in expressing the ideas included in this manuscript. Several colleagues have been invaluable resources for the development of this work, including Matthew Hiatt, Harish Sangireddy, and most of all Dr. Man Liang, who taught me how to use *DeltaRCM* and MATLAB, cultivated many of the concepts included here, and without whom this research would not be possible. I would also like to extend thanks to Dr. Matthew Wolinsky for graciously providing data for this project.

I am also very grateful to the engineering faculty at Calvin College, who taught me the importance of engineering as a vocation, inspired my excitement for learning, and demonstrated care for me as a student and as a person. In particular, I would like to thank Leonard De Rooy, Dr. Robert Hoeksema, and Dr. David Wunder for their impact on my education, career, and personal growth.

I also owe my friends and family a debt of gratitude for their continual support, encouragement, and prayers for me during my schooling and especially the past few years. Thank you for your love and concern.

Finally, I am thankful to the LORD for bringing me to Texas, for blessing me with the ability and opportunity for this work, and for His daily provisions of grace.

Abstract

Validation of a reduced-complexity numerical model for resolving deltaic dynamics: internal consistency and morphodynamics

Corey John Van Dyk, MSE

The University of Texas at Austin, 2015

Supervisor: Paola Passalacqua

River deltas are fragile ecosystems that have immense ecological, economic, and social importance. The ability to understand them is facilitated by numerical models that can resolve the complex hydrodynamics and morphodynamics of deltas. *DeltaRCM* is one such model, and to validate its behavior, internal consistency is tested with variable input parameters; results indicate realistic growth with predictable patterns. The morphodynamics are tested against experimental and real deltas with the use of metrics: specifically, delta growth metrics like shoreline-to-area ratio and relative shoreline roughness, channel overlap, and avulsion behavior. *DeltaRCM* performs very well when compared to real systems with growth rate and relative shoreline roughness, and fairly well for shoreline-to-area ratio. The channel overlap metric suggests *DeltaRCM* displays a slightly higher degree of channel stability than an experimental delta, though the general trend of memory decay remains the same. A similar link exists between *DeltaRCM* and reality for the wetted fraction, in that general trends are similar but

comparison breaks down at finer scales. Furthermore, based on *DeltaRCM* results, wetted fraction is an imperfect tool for determining avulsion timescale. A new metric, the sedimentograph, is introduced as a way of describing delta growth at the subsurface level; *DeltaRCM* gives reasonable results for this metric, though comparison to real systems is difficult.

Table of Contents

List of Tables

List of Figures

Chapter 1: Introduction

SIGNIFICANCE

The ability to explain and predict the behavior of any physical system is paramount in understanding how that system will affect society. River deltas warrant particularly rigorous analysis for several important reasons, as the net societal impact inherent in the geography, dynamics, and evolution of deltas is made up of a broad range of ecological, economical, and social effects. Understanding how deltas grow and transport matter will provide vital information for how humans should interact with deltaic environments in a responsible manner.

The ecological impacts that a delta has are perhaps the most obvious. Since most deltas form where a river meets the sea, the combination of fluvial forcings and oceanic forcings create several unique habitats for many plant and animal species to thrive [e.g. Cahoon et al., 2011]. The sediment deposition that occurs in deltaic systems also provides the nutrients necessary for tremendous biological productivity in both wetland and marine ecosystems [Rabalais et al., 1996; Qu et al., 2014].

The economic effects also highlight the importance of deltaic systems. Due to the sediment deposition and frequent flooding, the land within deltas tends to be fertile, facilitating agriculture [Ericson et al., 2006]. Due to the proximity of some deltas to ports, the shipping industry can affect and be affected by deltaic environments as well. More directly, the lucrative oil and gas industries are impacted by river deltas, since deltas are sometimes indicators of nearby hydrocarbon reserves.

Since nearly a half billion people live within river deltas [Syvitski & Saito, 2007], the social impacts of deltas can be enormous. Coastal wetlands, of which deltas are a part, provide a crucial buffer with regards to storm surge. The loss of wetlands, like that

of the Louisiana Gulf coast (Figure 1), highlights the danger of losing such a buffer near large population centers. An avulsion, when a channel changes direction due to significant sediment deposition in its current path, happen relatively frequently within deltas and can cause catastrophic damage [Rudra, 2014]. The quality of life for people living in deltaic environments could be drastically improved through understanding certain concepts like avulsive behavior or how sediment diversions can recreate land that has been lost (Figure 2).

Numerical models that accurately portray deltaic dynamics are especially important because of the limitations of field work and experimental deltas. Field work is time-consuming, arduous, and generally yields only information about one portion of one particular system. Because of the great diversity found in river deltas across the world (Figure 3), the analysis of many types of deltaic systems is imperative. Studying experimental deltas, especially when investigating how input parameters affect the growth characteristics, also involves significant time requirements, in addition to introducing spatial and temporal scaling issues. While numerical models cannot replace data gained from these "real-life" approaches, efficiency, ease with which parameters can be changed, and ability to study temporal changes make numerical modeling an important piece in studying deltaic systems.

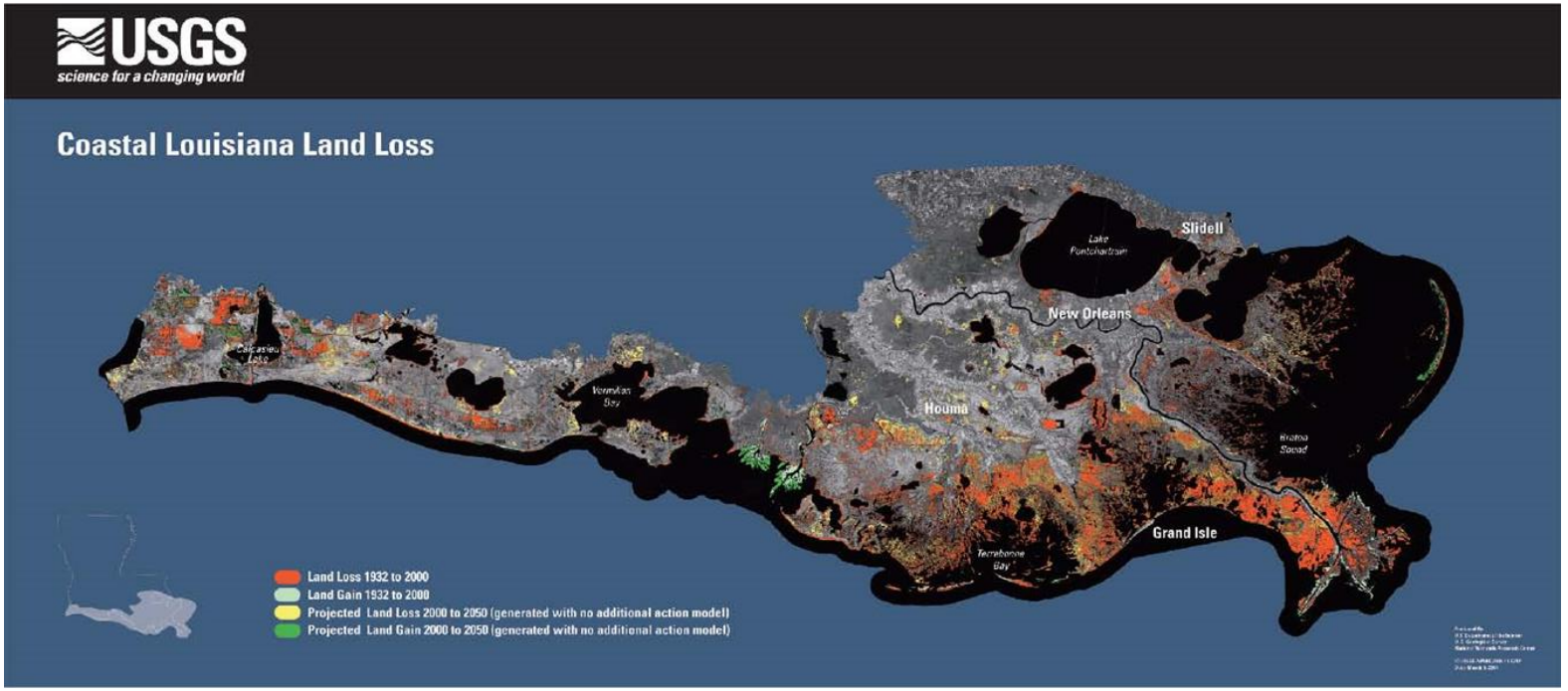

Figure 1: Historical and future land change map for Coastal Louisiana [USGS].

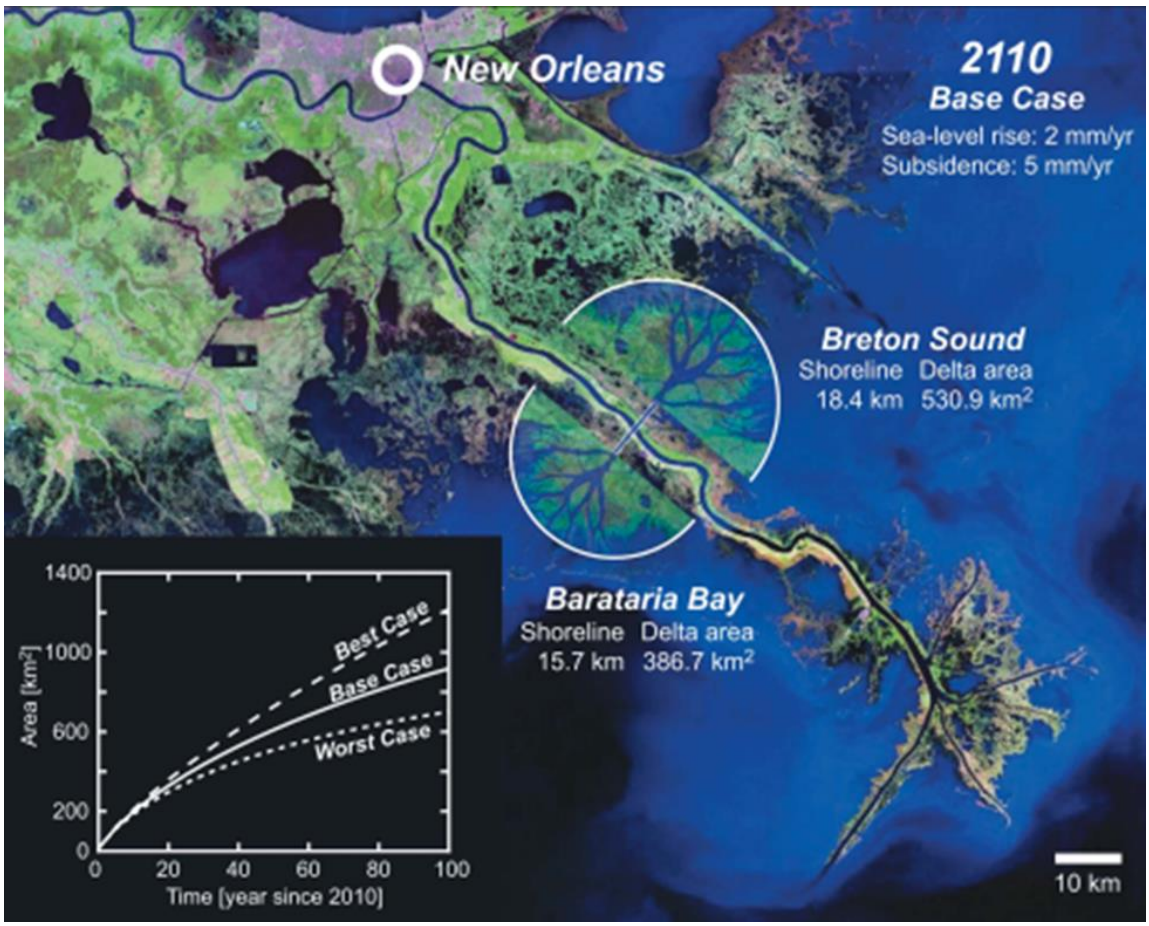

Figure 2: The Mississippi Bird's Foot Delta with two additional lobes created by theoretical sediment diversions [Kim et al., 2009].

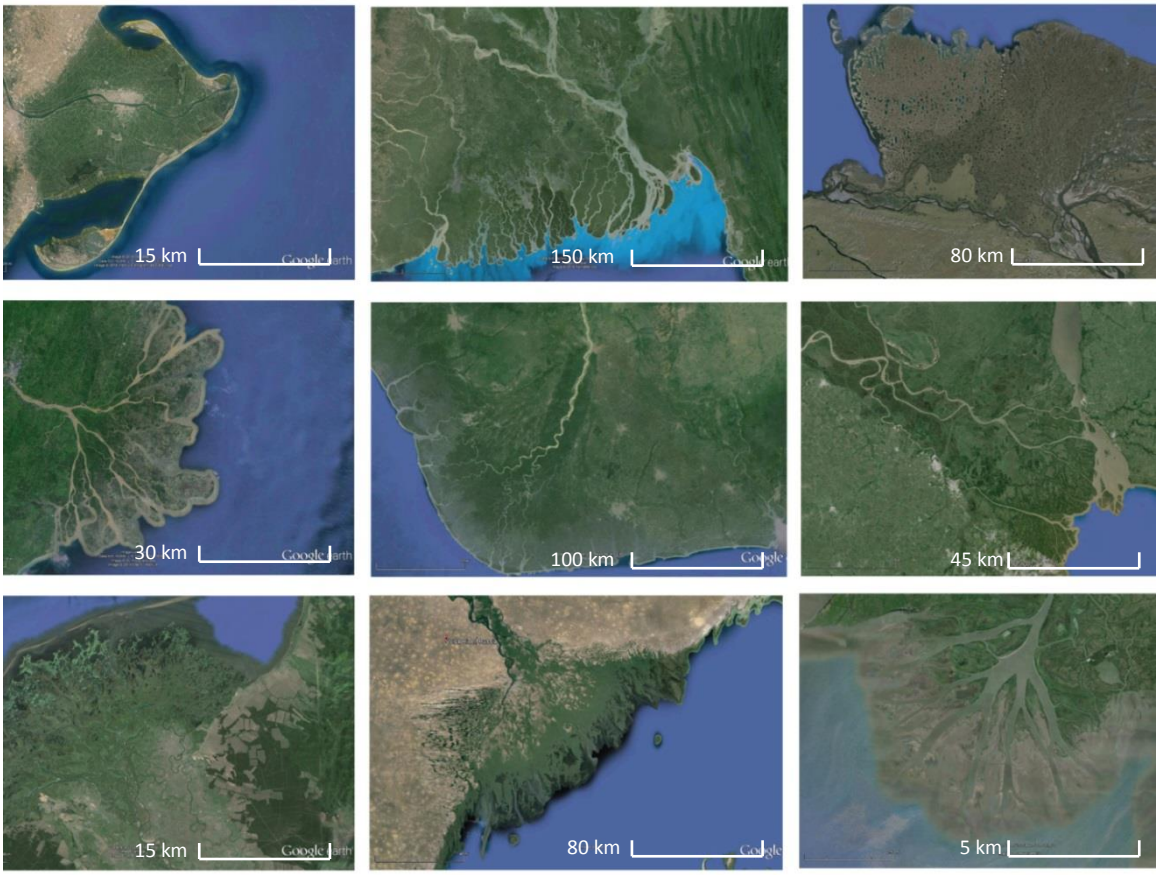

Figure 3: Several deltas with vastly different properties due to both autogenic and allogenic properties. Top (l-r): Ebro, Spain; Ganges-Brahmaputra, Bangladesh and India; Lena, Russia. Middle (l-r): Mahakam, Indonesia: Niger, Nigeria; Paraná-Uruguay, Argentina and Uruguay. Bottom (l-r): Selenga, Russia; Volga, Russia and Kazakhstan; Wax Lake, USA.

There is a spectrum of complexity regarding numerical models that can be used to simulate and study delta growth. One-dimensional models represent the lower end of this spectrum and are often based on spatial averaging of delta topography [Parker et al., 2008; Kim et al., 2009]. For resolving deltaic behavior with a multi-dimensional domain, models fall into one of two broad categories: high-resolution and reduced-complexity (Figure 4). High-resolution delta models resolve hydrodynamics and morphodynamics by solving theoretical relationships like forms of the Navier-Stokes equations. For example, Delft3D, the premier high-resolution model, solves the shallow water equations and empirical sediment transport formulas to determine water and sediment transport [Lesser, 2004]. Reduced-complexity models (RCMs), on the other hand, simplify the equations while retaining as realistic results as possible. The advantage of using RCMs is twofold: first, they are less computationally expensive than high-resolution models; second, the simpler methods used in determining water and sediment transport allow for a more intuitive understanding of the processes and facilitate changing input parameters. *DeltaRCM* falls into this latter category of models [Liang et al., 2015a].

Because they aren't entirely physics-based, RCMs need to be tested against real systems, at either experimental-scale or full-scale, to ensure realistic behavior. While hydrodynamic aspects can be tested against established theoretical relationships, the validation of morphodynamic behavior requires the development of robust metrics which can be measured for the model and real system for comparison.

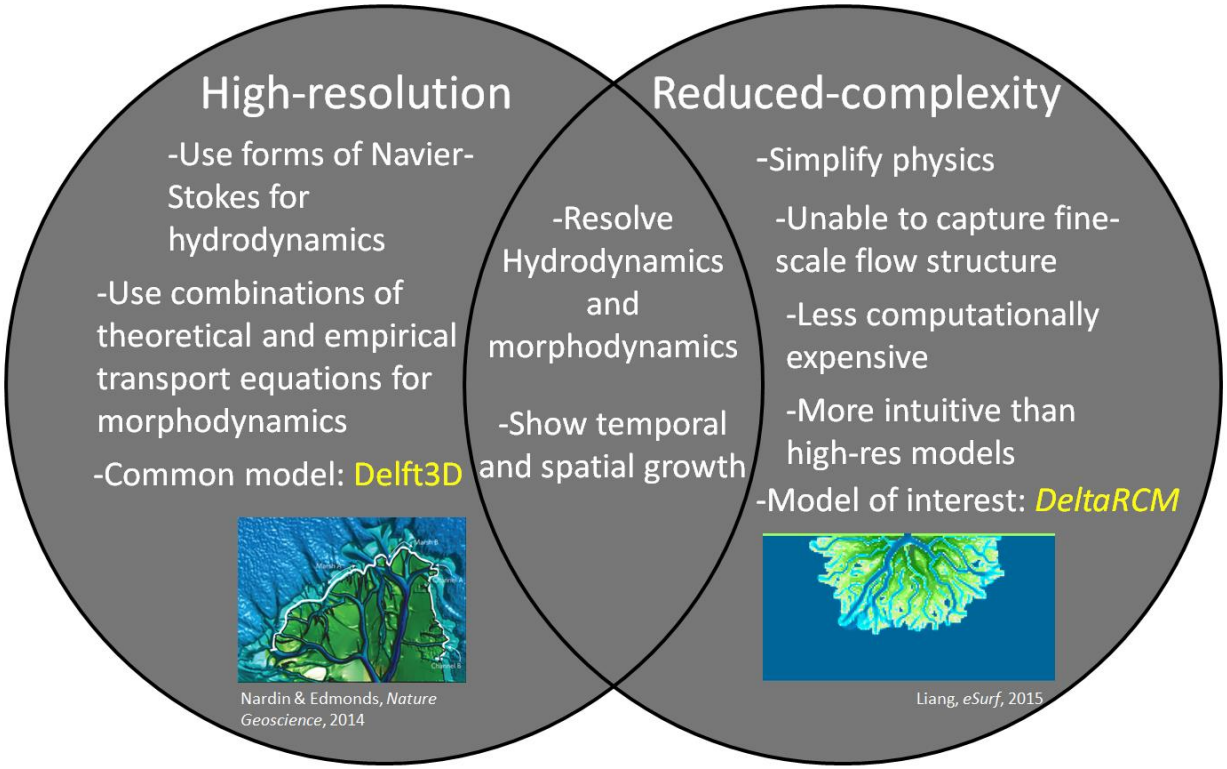

Figure 4: Venn diagram describing mechanism and capabilities of multi-dimensional hydro-morphodynamic models.

RESEARCH QUESTIONS

This project sought to answer the following questions:

1. Is *DeltaRCM* internally consistent in the way it predicts deltaic evolution?
2. Are the morphodynamics of *DeltaRCM* modeled in a realistic way, as compared to experimental setups and real deltas?

HYPOTHESES

The following hypotheses are put forth:

1. *DeltaRCM* models deltas in an internally consistent fashion, evidenced by distinct yet statistically similar results for runs with identical input parameters. Furthermore, changes in input parameters yield consistent changes in the resulting deltas.
2. *DeltaRCM* models the morphodynamics of deltas realistically at a network scale, shown by comparison to field-scale and experimental deltas by use of several metrics such as planform area growth, channel overlap, and avulsion characteristics.

Chapter 2: Literature Review

NUMERICAL MODELS

Numerical models have been used extensively to model deltaic behavior, varying from high resolution models like Delft3D [e.g. Edmonds and Slingerland, 2007; Edmonds et al. 2011; Caldwell and Edmonds, 2014] to simplified 1-D models based on spatial averages [Parker, 2008; Kim, 2009]. In between these extremes are RCMs, which have been used to model deltas in several instances. Seybold et al. (2007) used the shallow water equations like Delft3D, but simplified them by holding diffusivity constant. A model focusing on channel avulsion was developed by Sun et al. (2002) to replicate alluvial fan growth.

DELTARCM

DeltaRCM is a reduced-complexity model for river delta formation created by Man Liang [Liang et al., 2015a]. Using a "weighted random walk" method, the model directs water and sediment parcels through a lattice of square cells (Figure 5). This method balances physical processes with stochasticity to produce realistic deltaic systems. Inertia, water depth, surface slope, and sediment concentration are some of the physical rules that determine parcel transport. The water, sand, and mud parcels each follow their own sets of rules. The routing of water parcels is determined by water depth and the average downstream direction of flow in that cell. The routing of sediment parcels is a function of the water discharge vector (calculated for the associated water parcel) and water depth, with depth weighted more heavily for sand than for mud parcels. Empirical laws, distinct for mud and sand, are used to determine deposition rates; erosion rates are determined by threshold for local flow velocity. Further information about how *DeltaRCM* works can be found in Liang et al. (2015a).

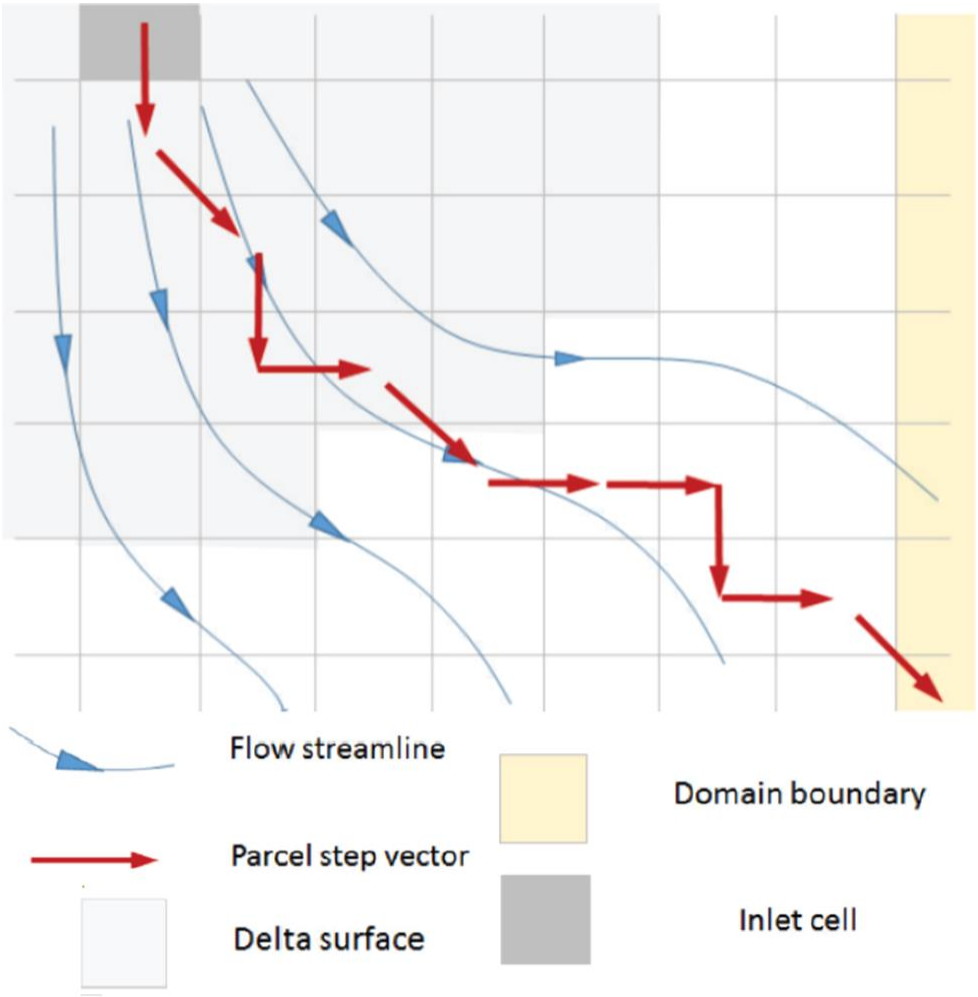

Figure 5: Schematic showing how water and sediment parcels are transported through *DeltaRCM* [Liang et al., 2015a].

The first step in validating *DeltaRCM* was analyzing the hydrodynamics. Liang et al. (2015b) compares the model's performance against the backwater equation and Delft3D, which solves the shallow water equations. Figure 6 shows how *DeltaRCM* models the backwater curve perfectly, as well as how velocity contours compare to Delft3D at two different scales. Due to the cellular nature of *DeltaRCM*, the water upstream of the bifurcation (the lower left section of Figure 6) has no "knowledge" of the divergence, and therefore models the bifurcation less accurately than Delft3D, where the shallow water equations "inform" the upstream water of the impending junction. On the network scale, however, these discrepancies become less pronounced, and the velocity pattern created with *DeltaRCM* matches with Delft3D fairly well. More discussion on *DeltaRCM*'s hydrodynamic validation can be found in Liang (2015b).

MORPHODYNAMIC METRICS

Because sediment transport, deposition, and erosion lack a comprehensive theoretical relationship like the Navier-Stokes equations that can be used to validate a model's performance, other methods must be developed by which comparisons to experimental and real deltas can be made. These comparisons require metrics that describe some morphodynamic characteristic of a system that can be recorded by the model as well as measured in a real or experimental scenario.

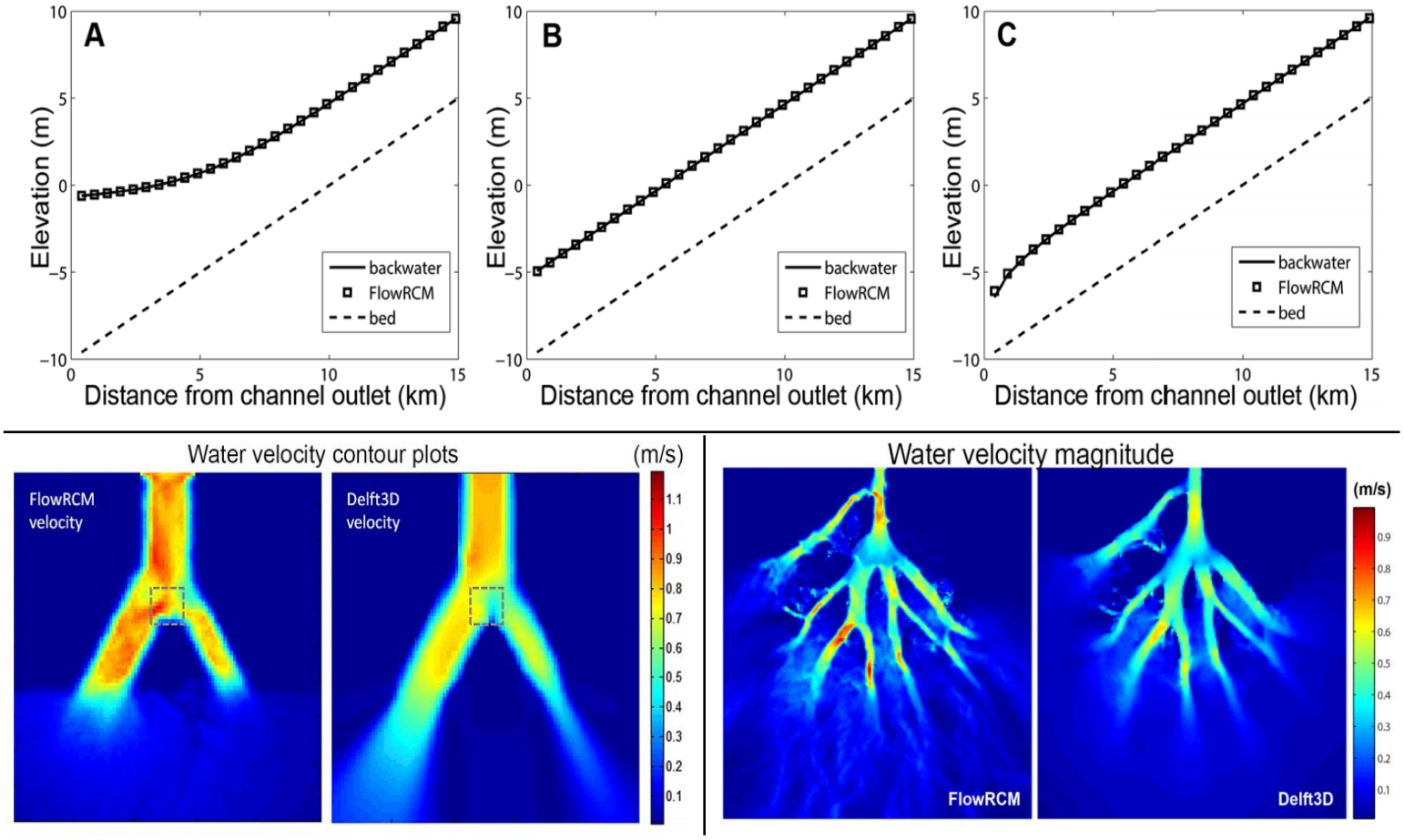

Figure 6: Top: Water surface (l-r: M1, normal, M2) as calculated with the backwater equation and determined from *DeltaRCM*. Left: Water velocity at bifurcation, as determined by *DeltaRCM* and Delft3D. Right: Water velocity in Wax Lake Delta, as determined by *DeltaRCM* and Delft3D [Liang et al., 2015b].

There has been some, though not copious, research done regarding morphodynamic metrics both derived from field data and experimental setups. Wolinsky, et al. (2010) analyzed delta allometry, focusing on land area, wetted area, shoreline length, and wetted edge-length, for field-scale, experimental, and numerical deltas. Fractal dimension, synthetic sediment flux, and nourishment area (the distributary analog to contributing area) were some of the metrics studied in Edmonds, et al. (2011). These were also analyzed with respect to theoretical, experimental, and actual river deltas. Passalacqua, et al. (2013) focused on the Ganges-Brahmaputra delta and examined metrics like island area, island shape factor, nearest-edge distance, and oxbow density. Several other studies have studied the morphodynamics of river networks and describe trends in delta evolution without explicitly identifying metrics. For example, Shaw et al. (2013) examined how channel erosion incises the pre-delta substrate and showed how transfer into the islands was a significant factor in sediment transport. Reitz & Jerolmack (2012) delved into the flow paths that channels select in alluvial fan deltas. They used an experimental fan delta to model the avulsion behavior, which was also demonstrated with a numerical model. Also discussed was how the wetted area changes over time and its relationship to avulsions.

Chapter 3: Methods

RUNS

Seven different runs were performed, with each set of input parameters triplicated for a total of twenty-one runs (Table 1). Obtaining a wide variety of delta types was achieved by varying sand fraction from 10% to 90% and varying basin depth from 2.5 meters to 10 meters. For each run, the inlet channel depth was 5 meters, the inlet channel velocity was 1 meter per second, the cell size was 50 meters square, and the width of the inlet channel was 5 cells. The characteristic topographic slope, which is the channel slope and the slope the forming delta will take, is a function of the sand fraction and is given by:

$$S = 0.0003 * f_{sand} + 0.0001 * (1 - f_{sand}), \quad (1)$$

where f_{sand} is the sand fraction. These values were determined to reasonable bounds of 10-4 for purely mud deltas and 3×10-4 for purely sand deltas.

DATA EXTRACTION

In order to obtain some of the metrics used for comparison, some additional data had to be extracted from the model results. *DeltaRCM* gives bed elevation and water depth, velocity, and discharge (Figure 7). However, the processes used to extract the delta shoreline and planform area warrants further discussion.

Table 1: List of runs performed.

Run Number	Designation	Basin Depth (m)	Sand Fraction
1	standard 01	5.0	30%
2	standard 02	5.0	30%
3	standard 03	5.0	30%
4	10_sand 01	5.0	10%
5*	10_sand 02	5.0	10%
6*	10_sand 03	5.0	10%
7	50_sand 01	5.0	50%
8	50_sand 02	5.0	50%
9	50_sand 03	5.0	50%
10	70_sand 01	5.0	70%
11	70_sand 02	5.0	70%
12	70_sand 03	5.0	70%
13	90_sand 01	5.0	90%
14	90_sand 02	5.0	90%
15	90_sand 03	5.0	90%
16	shallow 01	2.5	30%
17	shallow 02	2.5	30%
18	shallow 03	2.5	30%
19	deep 01	10.0	30%
20	deep 02	10.0	30%
21	deep 03	10.0	30%

*Did not yield complete results; see “Data Extraction” for explanation.

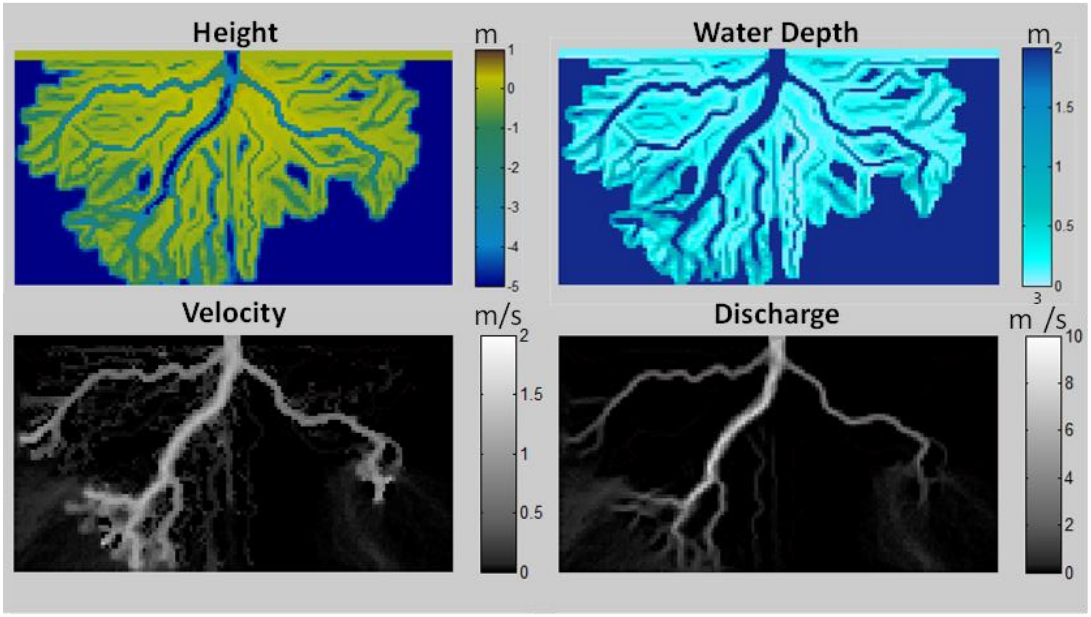

Figure 7: Height, water depth, water velocity, and water discharge during the last time step of a delta run.

As described in Shaw et al. (2008), the opening angle method was used to determine the shoreline placement. First, a binary map of the delta was created, separating subaerial (land) pixels from subaqueous (water) pixels. Next, an "opening angle" is computed at each pixel by measuring the largest possible angle through which only water can be "seen" (Figure 8). If the angle is less than a threshold value (in this case, 45°), that pixel is declared land; if greater than the threshold, the pixel is sea. The border between is the shoreline. Until about 10% into each run, not enough land had been constructed to create a shoreline that reached the upper edge of the basin, so these beginning time steps were disregarded by necessity. For two of the runs with 10% sand (runs 5 and 6), the delta land never reached the edge, and the shoreline was not completed at all.

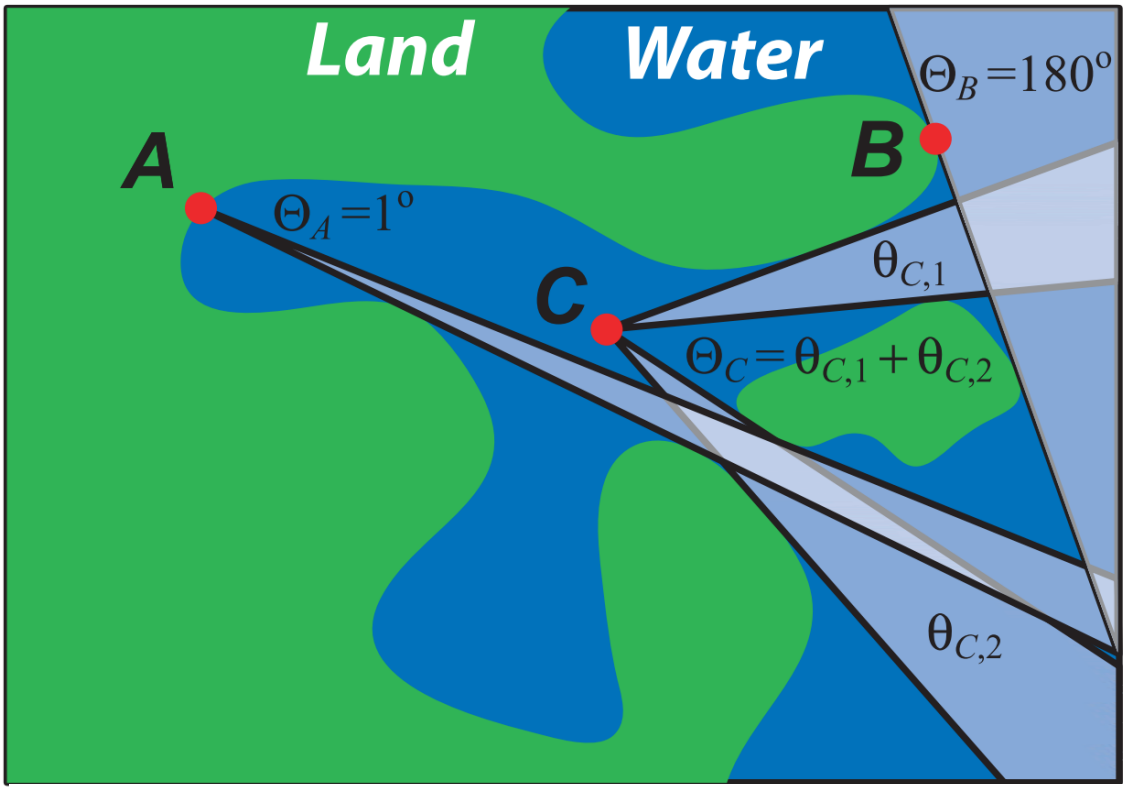

Figure 8: Several options for using the opening angle method [Shaw et al., 2008].

The domain boundary pixels are unable to "see" land and are declared shoreline by the algorithm (Figure 9a). Conversely, pixels near the inflow "see" only water when looking upstream, so a shoreline is created between these pixels and the bulk of the delta (Figure 9b). These false shorelines are removed (Figure 9c), and the delta is filled in to define the planform area (Figure 9d). For runs 5 and 6, since the shoreline was incomplete, the delta was unbounded and step (d) could not measure the planform area.

By implementing a discharge or velocity threshold, binary maps of active channels were obtained, as shown in Figure 10. Unless noted otherwise, the discharge threshold of 0.5 cubic meters per second was used to define the active channels, as it generally gave the maps with the least noise while retaining the channel network.

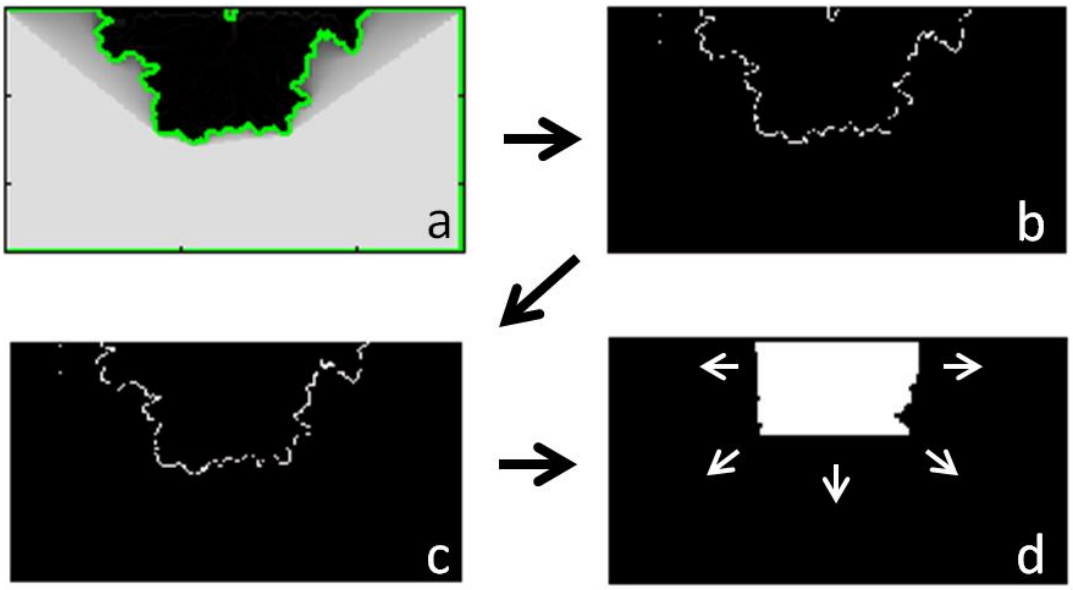

Figure 9: Shoreline extraction process: (a) The opening angle method is used over the whole domain; the (b) domain boundaries and (c) apex area are removed, and (d) pixels fill in the delta from the apex to the shoreline, thus creating the planform area (arrows indicate expansion of area up to shoreline for each time step).

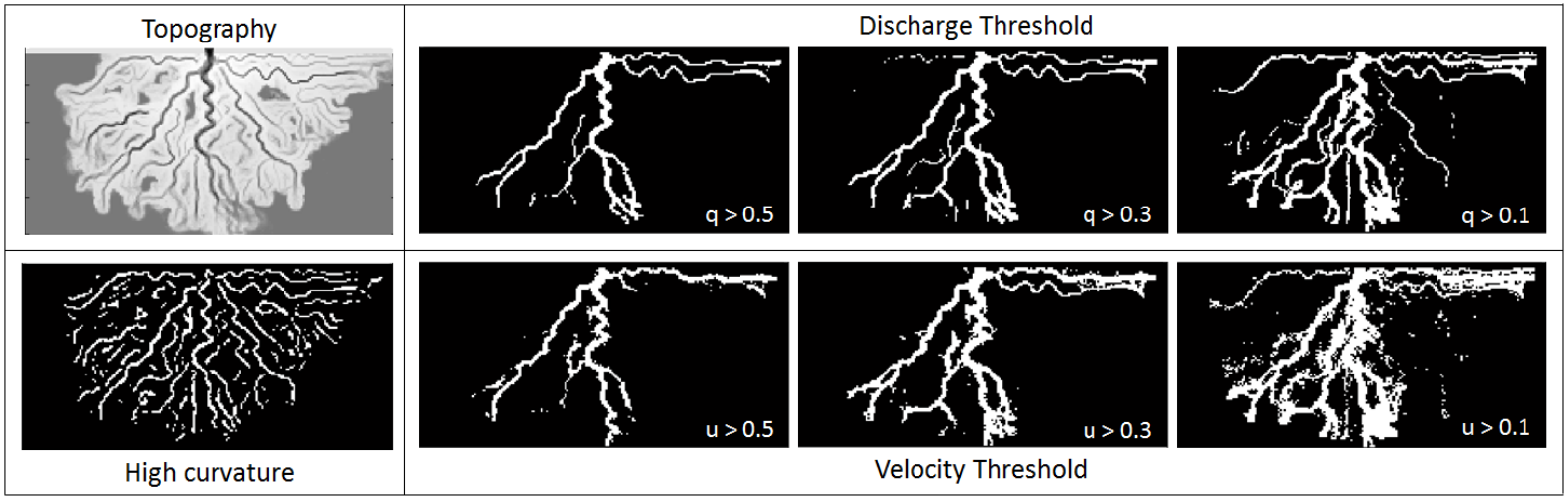

Figure 10: Top (l-r): Topography of a delta used as reference for other images; binary maps of active channels with discharge thresholds as shown. Bottom (l-r): Binary map of all channels (active and inactive) as determined by curvature threshold; binary maps of active channels with velocity thresholds as shown.

INTERNAL CONSISTENCY

Three techniques were used to test for internal consistency. First, by keeping input parameters constant, identical runs were performed to determine if the resulting deltas would be statistically similar yet not identical due to stochastic processes. Second, by varying sand fraction and depth, changes in results were found to be consistent with changes in input parameters, in ways that could be expected based on deltaic dynamics. Third, growing deltas were observed through time to ascertain that they evolve in a steady manner, with basic properties like bulk shape and incremental areal changes remaining consistent.

These characteristics were compared primarily by visual analysis of delta maps, though quantitative analysis of shoreline roughness and delta age (how long a pixel has been part of the delta area) was performed as well.

METRIC COMPARISON

Metric Suite

Due to the relatively scarce amount of research that has been done on morphodynamic metrics, a set of metrics, or "metric suite" was developed which would facilitate morphodynamic validation for *DeltaRCM* as well as act as a reference for other modelers [Liang et al., 2015c]. Table 2 lists these metrics while categorizing them by type and location within the delta. Several of these metrics are discussed in the following sections.

Table 2: Metric suite.

	Surface/Sub-aerial				Subsurface/Sub-aqueous	
	Island	Channel	Shoreline	Topset	Foreset and bottom-set	Stratigraphy
Bulk geometry and topology		Fractal dimension; Wetted fraction; Wetted edge length	Rugosity; Number of channel mouths	Area; Shape; Slope	Area; Slope	Sedimentograph
Spatial distribution	Nearest edge distance; Island size; Island shape; Oxbow-lake density	Channel width; Channel section length; Channel sinuosity; Bifurcation angle; bifurcation asymmetry; Bifurcation intensity				Variogram; Sand body shape; Sand body connectivity
	Nourishment area; Synthetic sediment flux					
Temporal distribution		Avulsion timescale; Channel instantaneous planform change; Channel planform overlap; Channel reworking timescale				Compensation index

Delta Growth Metrics

Three delta growth metrics computed from *DeltaRCM* data were compared against data gathered by Wolinsky et al. (2010). Numerical model data was generated by Delft3D, experimental data was created with the Jurassic Tank at St. Anthony Falls Laboratory (SAFL) at the University of Minnesota Twin Cities (using a "weakly cohesive sediment mixture"), and satellite images were recorded of Mossy Delta in Cumberland Lake in Saskatchewan (Figure 11).

The first metric was planform area. This area includes all the land and water bounded by the delta shoreline. To facilitate comparison between deltas of different scales, area and time were normalized by the final area and final time, respectively. The second metric analyzed was the ratio of shoreline length (normalized by final length) to planform area (normalized by final area). Relative shoreline roughness was studied as the third metric, shown as it progresses through time and given by

$$R = \frac{shoreline\ length}{\sqrt{planform\ area}}. \quad (2)$$

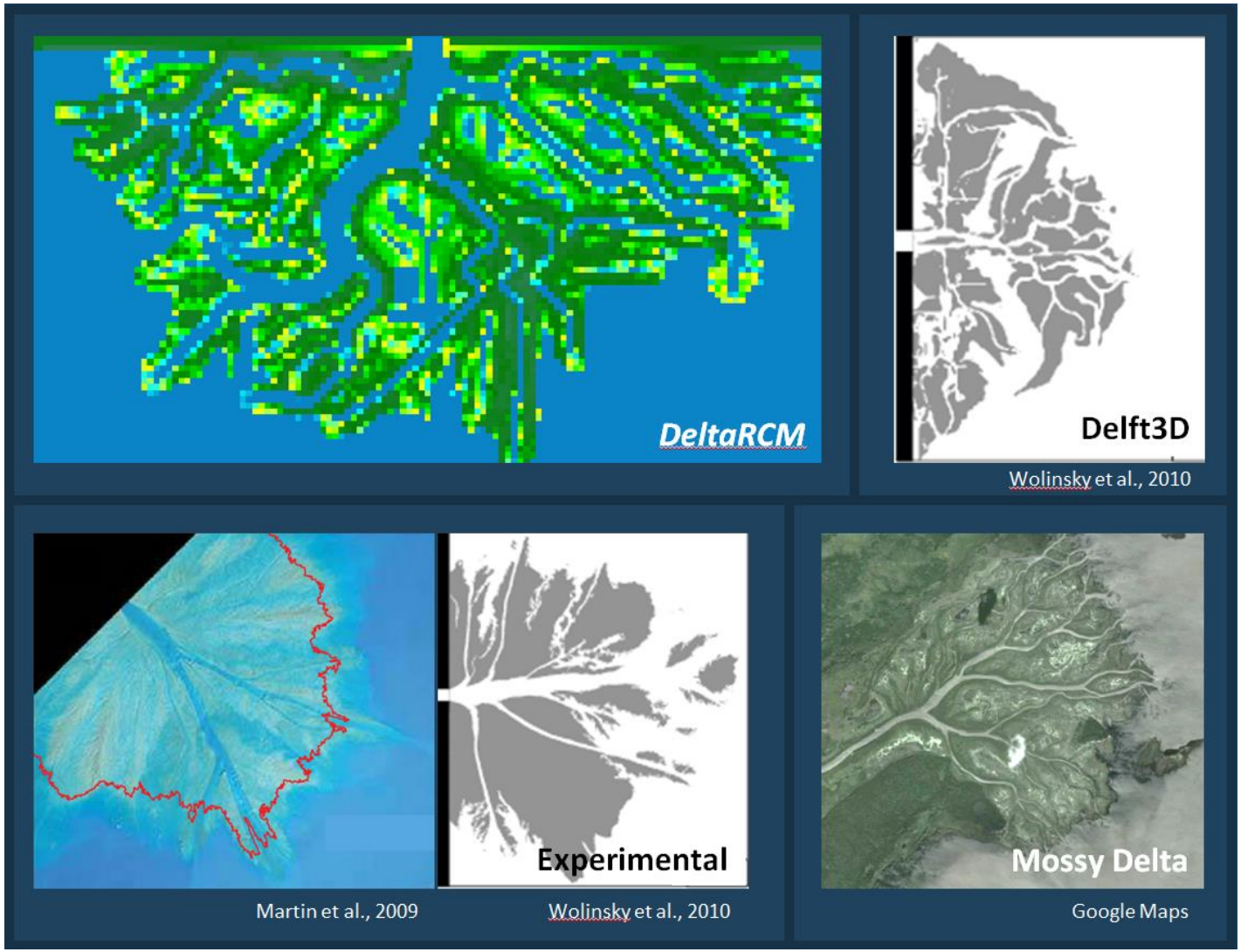

Figure 11: Four datasets with which delta growth was compared.

Channel Overlap

The degree of channel migration that occurs during delta growth was captured by channel overlap as described in Wickert et al. (2013). Channel overlap refers to how similar a specified binary channel baseline map of the delta is to subsequent maps. This value is normalized by the delta area and a parameter which represents the amount of change if the map were randomized. In equation form, the difference is given by

$$D(B,T) = \sum_{i=1}^{m_r} \sum_{j=1}^{n_c} |K_B - K_T|, \tag{3}$$

where K is a binary channel map, B refers to the base value, T refers to a later time, and m_r and n_c are the numbers of rows and columns, respectively. The random scatter parameter is defined as

$$\Phi = f_{w,B} * f_{d,T} + f_{d,B} * f_{w,T}, \tag{4}$$

where f_w is the wet (occupied channel) fraction and f_d is the dry (land, unoccupied channel) fraction. Φ is the number of pixels that would change from B to T if the same wet and dry fractions were scattered randomly across each fluvial surface [Wickert et al., 2013]. Finally, the channel overlap is given as

$$O_\Phi = 1 - \frac{D}{A * \Phi}, \tag{5}$$

where A is the area of the fluvial surface (wet and dry), and D and Φ are defined above.

Comparing the baseline map to itself would produce no difference and yield an overlap value of 1. An overlap value of 0 implies a difference that is statistically random. The rate at which the overlap value decays over time relates to how long of a memory the system has in terms of channel reworking. Wickert et al. (2013) include a very useful schematic (Figure 12) that illustrates how the channel overlap works on a very small domain.

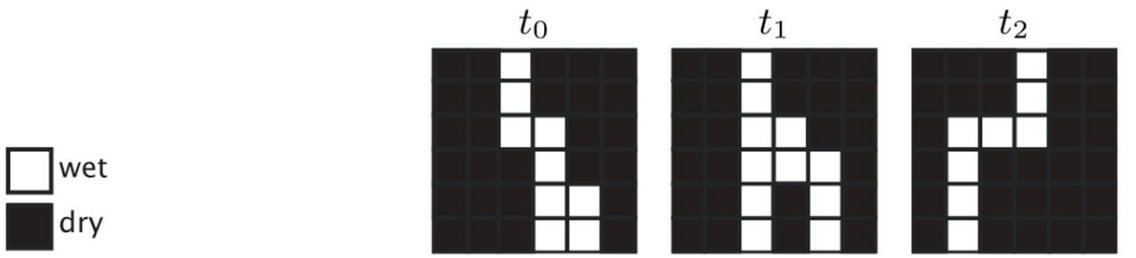

f_w	0.250	0.306	0.222
$D\left(B=t_0,T\right)$ (Eq. 1)	0	6	13
$D\left(B=t_0,T\right)/A$	0	0.167	0.361
Φ (Eq. 2)	0.375	0.403	0.403
O_Φ (Eq. 3)	1	0.586	0.104

Figure 12: Schematic demonstrating channel overlap equations [Wickert et al., 2013].

Wickert et al. (2013) presents several experimental datasets for comparison, including work performed by Kim et al. (2006) at the Jurassic Tank at SAFL, which served as the comparison to DeltaRCM.

Avulsion Behavior

When the sediment deposition in an active channel arrives at the point where it is energetically favorable for the channel to make a new route, this avulsion occurs over a relatively short time period and is fairly noticeable when looking at flow patterns given by DeltaRCM (Figure 13). However, manual examination of the flow paths can be tedious, so the "wetted fraction" is used as a proxy.

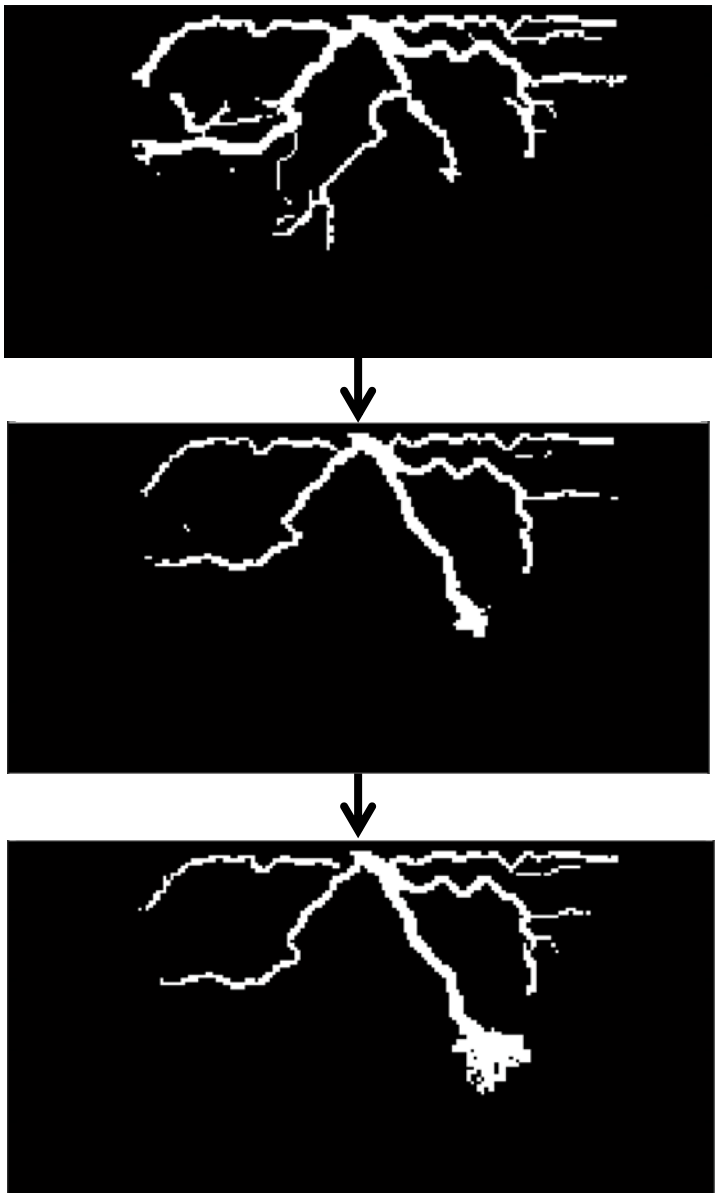

Figure 13: Three subsequent time steps showing an avulsion. Flowpaths are defined by discharge greater than 0.5 m^3/s.

The wetted fraction is the ratio of active channels (as shown in Figure 10) to the total surface area of the delta. Wetted fraction is a reasonable metric by which to examine avulsions because before an avulsion occurs, the delta slowly gets more and more flooded due to deposits inhibiting the water from flowing out, thus increasing the wetted fraction. When an avulsion occurs, the new channel drains the delta of excess water, leading to a sharp decrease in the wetted fraction.

The avulsion time can be extracted from a wetted fraction plot by determining the horizontal distance between two peaks (Figure 14). The time steps on the horizontal axis refer to about 70 hours of bank-full flood. Assuming bank-full flood occurs ~1% of the time, or 87.6 hours per year, these time steps coincide with about 0.80 years.

Avulsion behavior was compared against data from an experimental delta analyzed by Reitz & Jerolmack (2012).

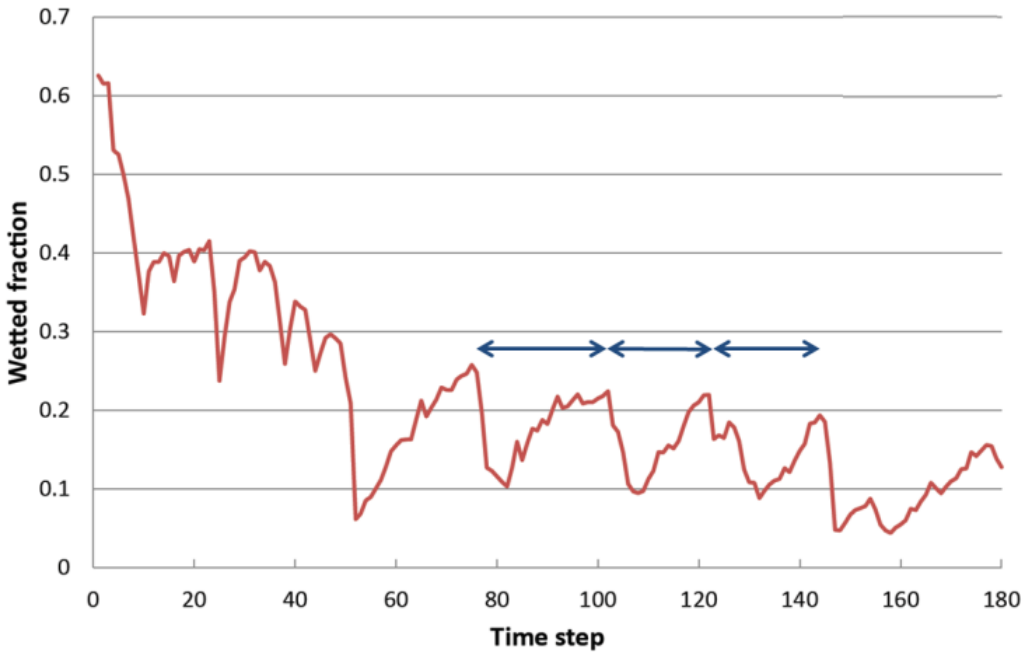

Figure 14: Wetted fraction plot demonstrating how avulsion timescale is estimated.

SEDIMENTOGRAPH

Despite the presence of the metrics above, a crucial aspect of understanding how deltas evolve would be missing if the subsurface were not examined. A new metric, called the sedimentograph, was introduced to capture the structure and dynamics under the surface. The sedimentograph uses a spatial average for the deposits to determine what kind of deposition occurs and where and how it changes temporally. Semicircular transects (like those shown in Figure 15) are cut into the delta at increments of one grid cell, and for each transect, an average sand fraction is computed. Sedimentographs change through time for a given delta and can offer insight into how the delta grows.

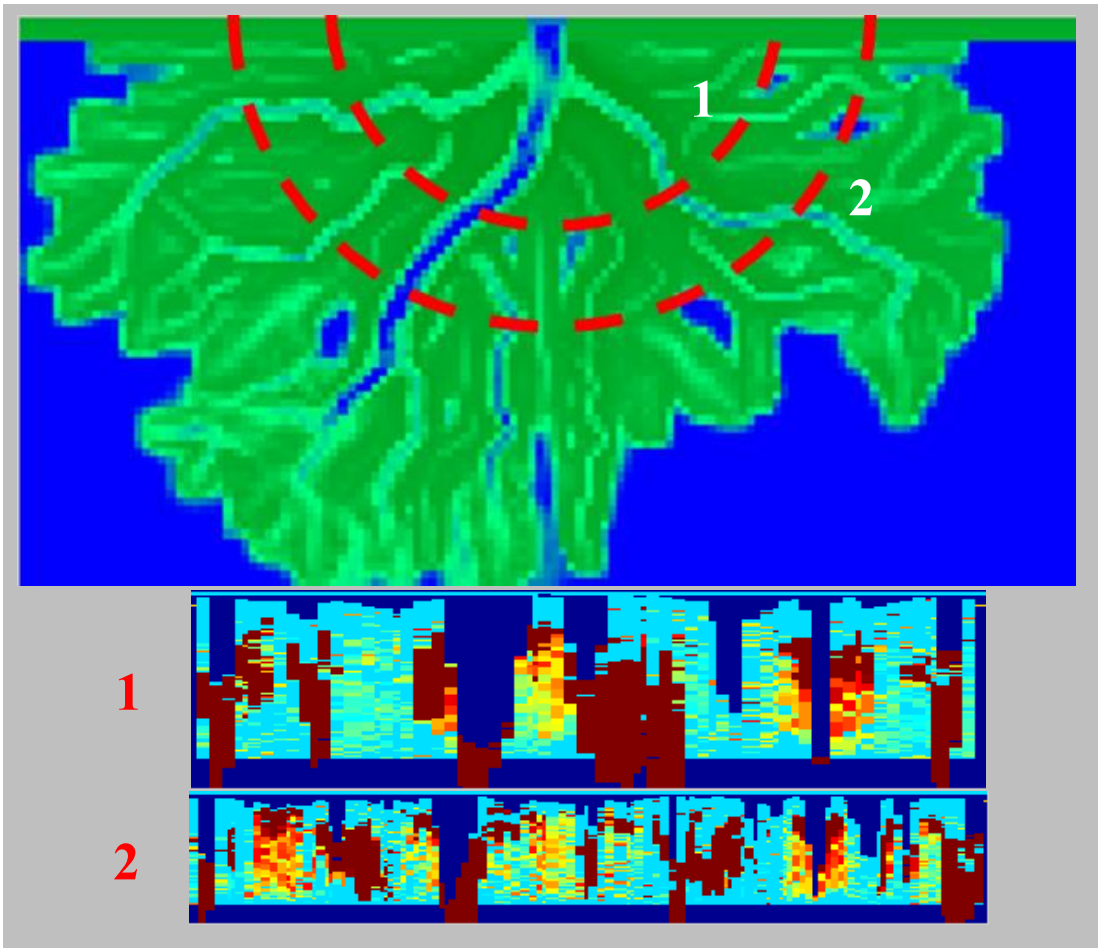

Figure 15: Delta with sample transects showing where the deposits are measured. In the transects, red means a high percentage of sand and blue means low.

Chapter 4: Results

Internal Consistency

The topography of the last time step and the delta age of runs 1, 2, and 3 (basin depth = 5.0 m; sand fraction = 30%) were investigated for internal consistency (Figure 16). The same was done for runs 10, 11, and 12 (basin depth = 5.0 m; sand fraction =70%) (Figure 17), while Figure 18 depicts runs 16, 17, and 18 (basin depth = 2.5 m; sand fraction = 30%). Characteristics of the topography and the delta age remain similar for runs with identical input parameters. For both sets with 30% sand, the final topographies appear to have one or two primary channels (based on its depth), with the other channels playing a less important role or even appearing disconnected from much of the delta. Elongate channels with levees are common, since the relatively high mud fraction is characterized by high cohesiveness. Figure 17, on the other hand, displays many channels that appear to be approximately equal in depth. Inter-channel islands are more clearly formed, and the shoreline has a much more semicircular shape. The plots of delta age are gradients also in the shape of semicircles, indicating that the delta grew at the same rate in all directions. The plots in Figures 16 and 18, on the other hand, show that the delta age is not as steady with low sand fractions, evidenced by distinct boundaries between colors. These well-defined borders indicate that the delta was not growing in that direction for a long time, perhaps avulsing in another. Finally, Figures 16 and 18 show that basin depth does not seem to have a large effect on the shape and direction a delta grows.

Results of runs with varying sand fraction are recorded in Figure 19. Figure 20 shows similar results, but for changing basin depth. Figure 19 depicts levees disappearing, the shoreline becoming smoother, and channels sharing flow more equally as sand fraction increases. Varying depth does not give a strong noticeable trend.

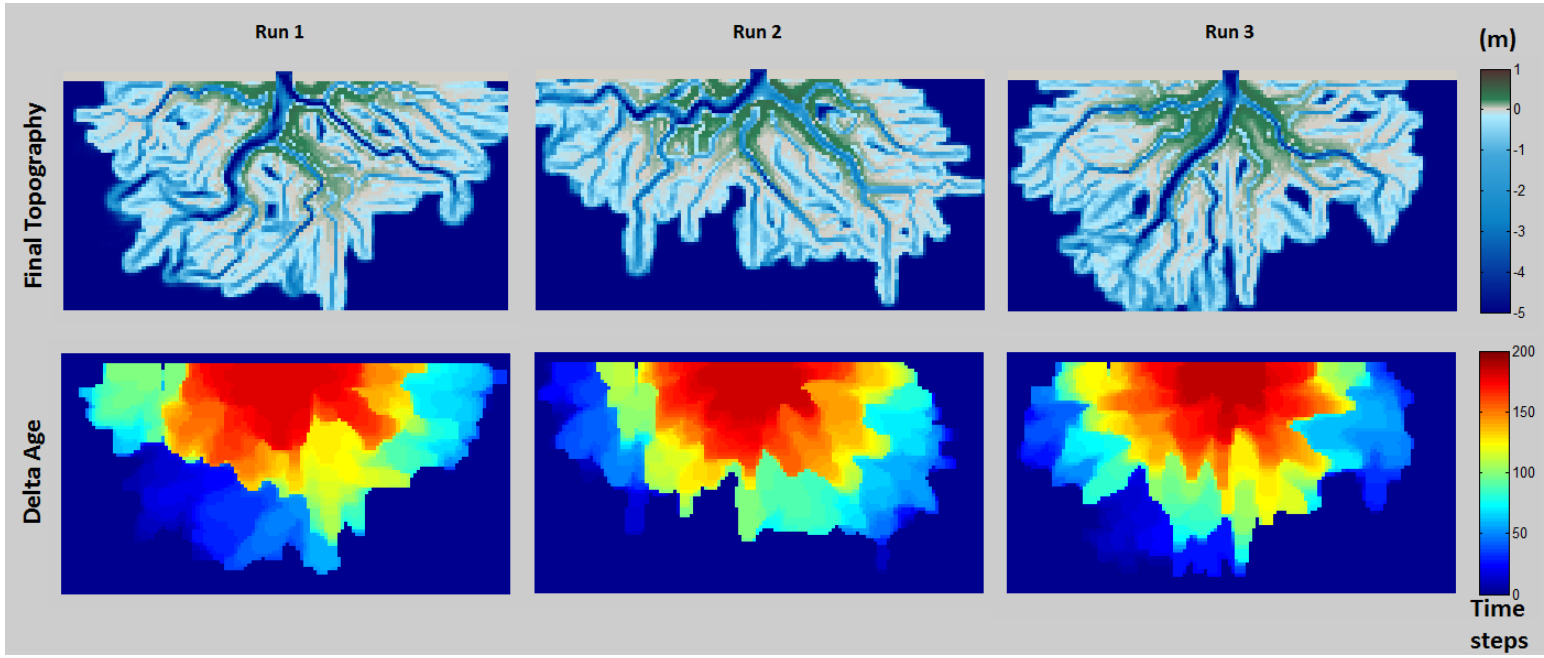

Figure 16: The topography of the final time step and the delta age for three runs created with a 30% sand influent and a 5.0 meter deep receiving basin.

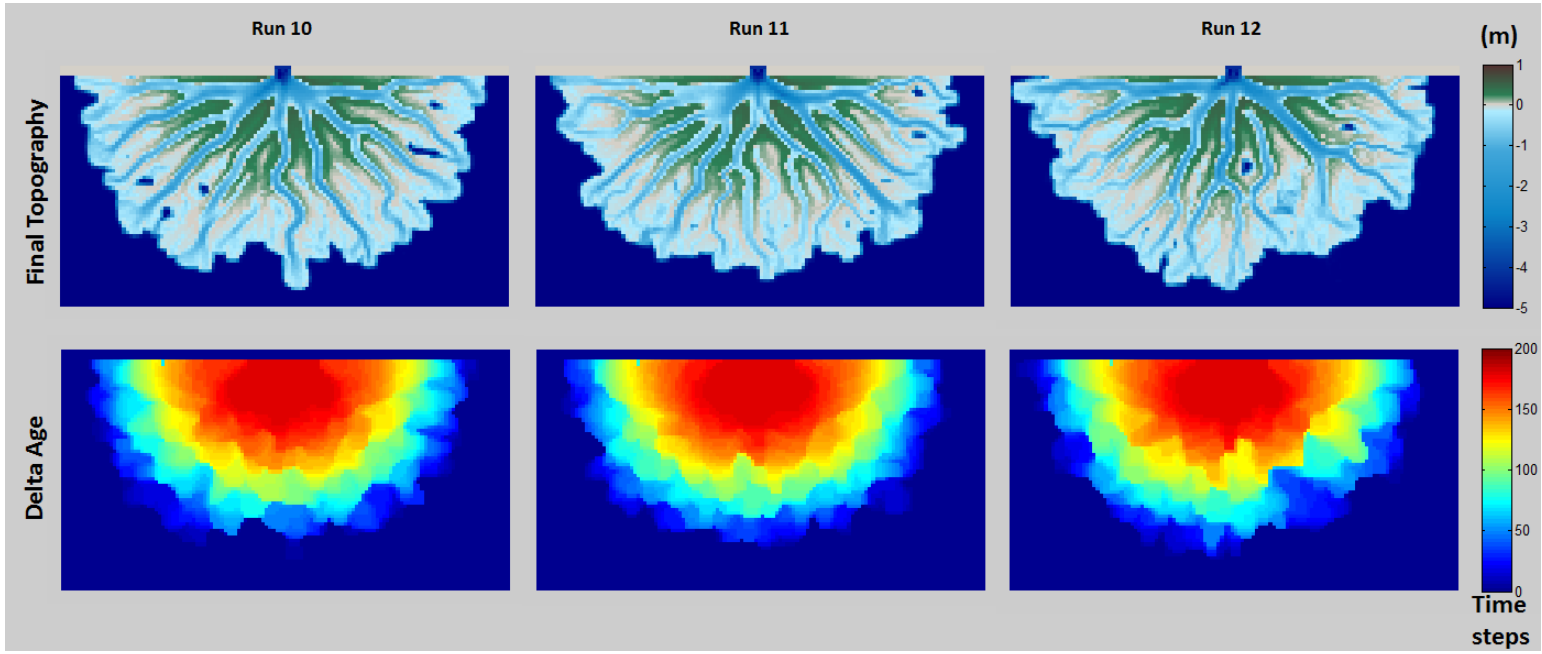

Figure 17: The topography of the final time step and the delta age for three runs created with a 70% sand influent and a 5.0 meter deep receiving basin.

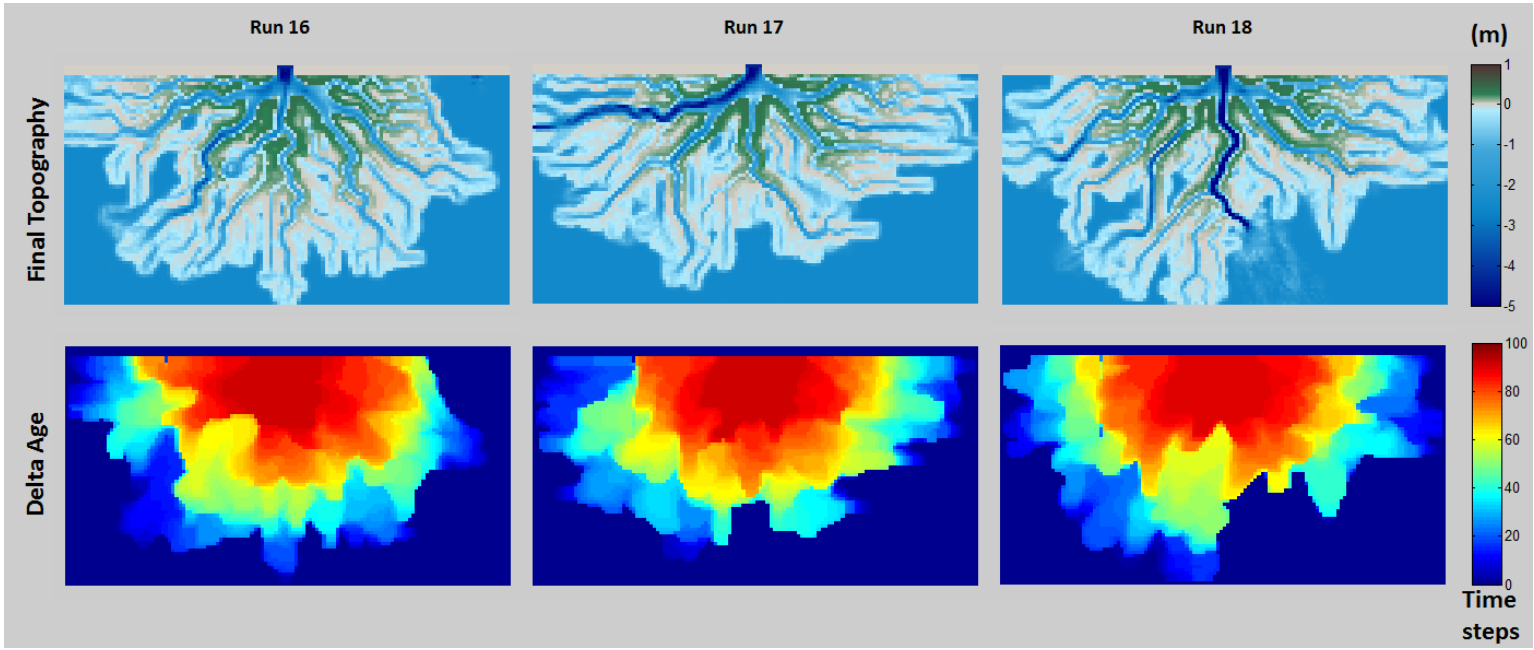

Figure 18: The topography of the final time step and the delta age for three runs created with a 30% sand influent and a 2.5 meter deep receiving basin.

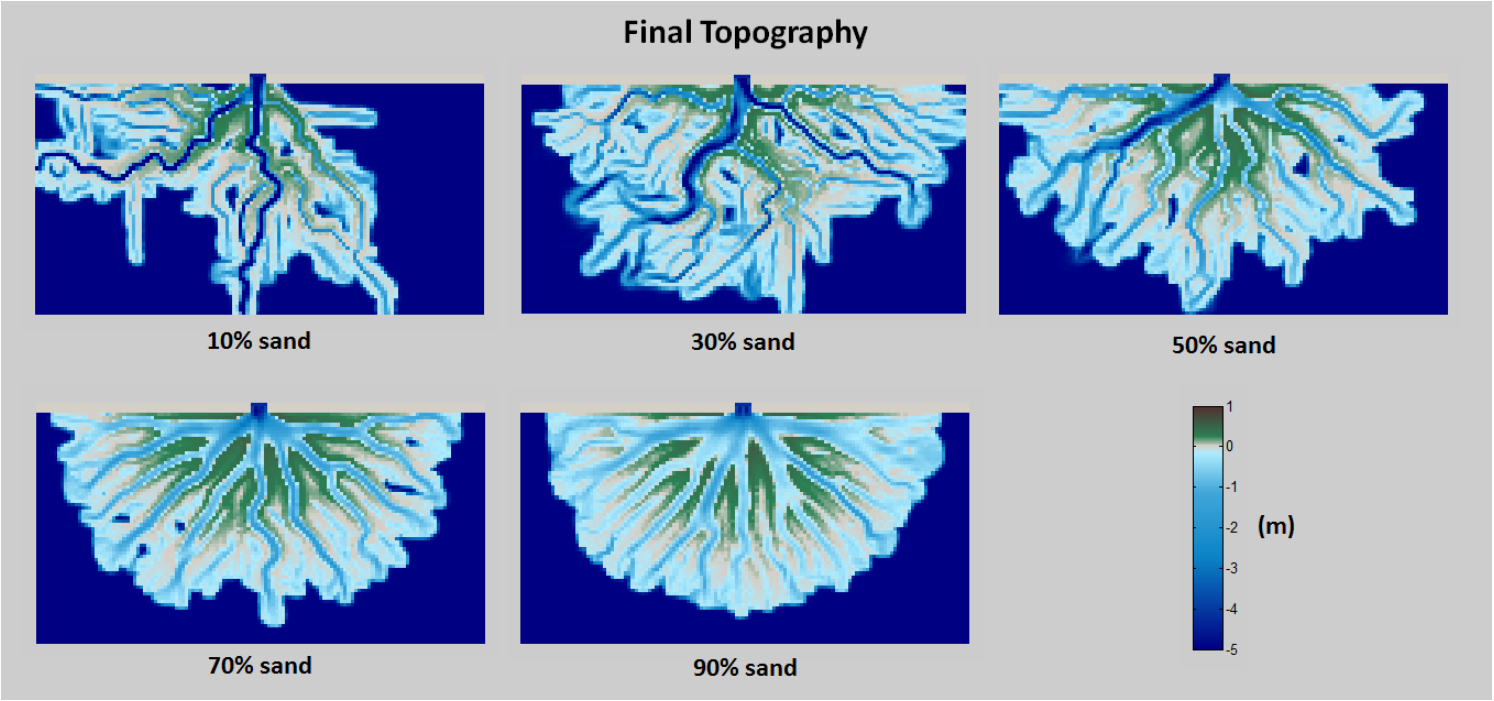

Figure 19: The topography of the final time step with varying sand fraction influents.

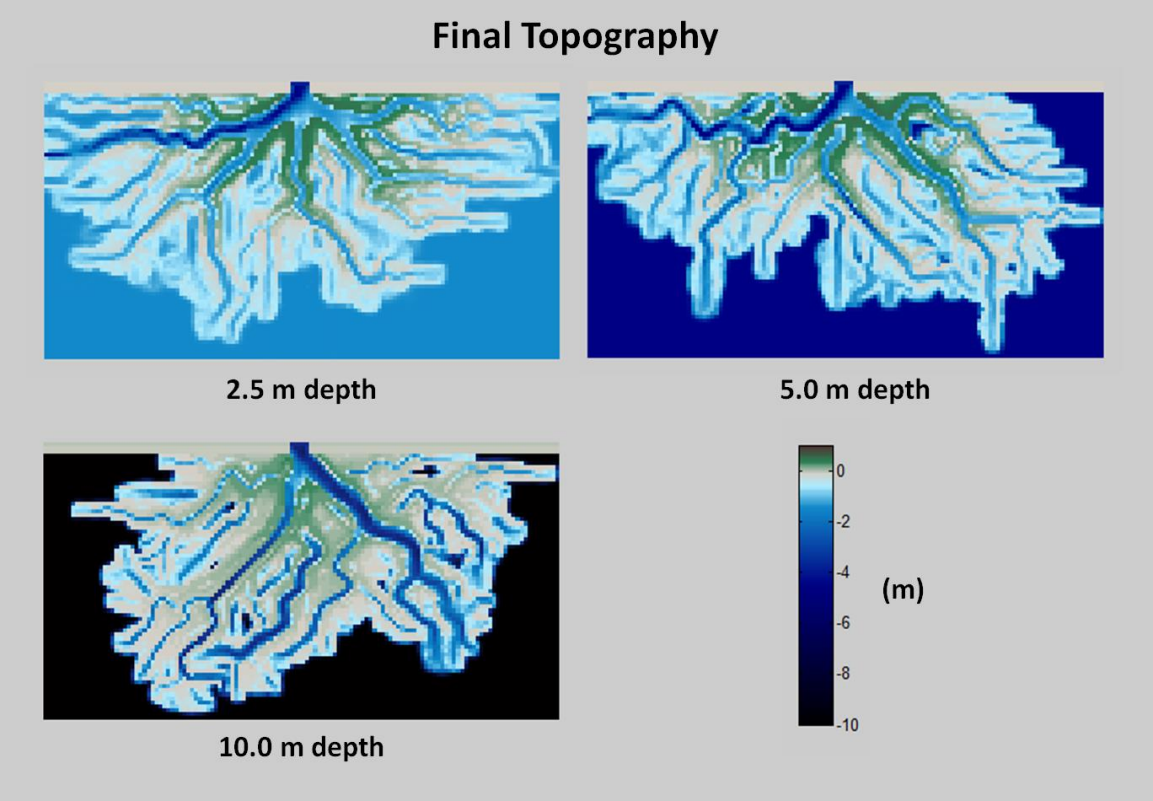

Figure 20: The topography of the final time step with varying basin depth.

Delta growth through time within three given runs (30% sand, 5 m; 90% sand, 5 m; 30% sand, 2.5 m) was mapped (Figure21). The structure and behavior of the delta remains remarkably similar through time for each run.

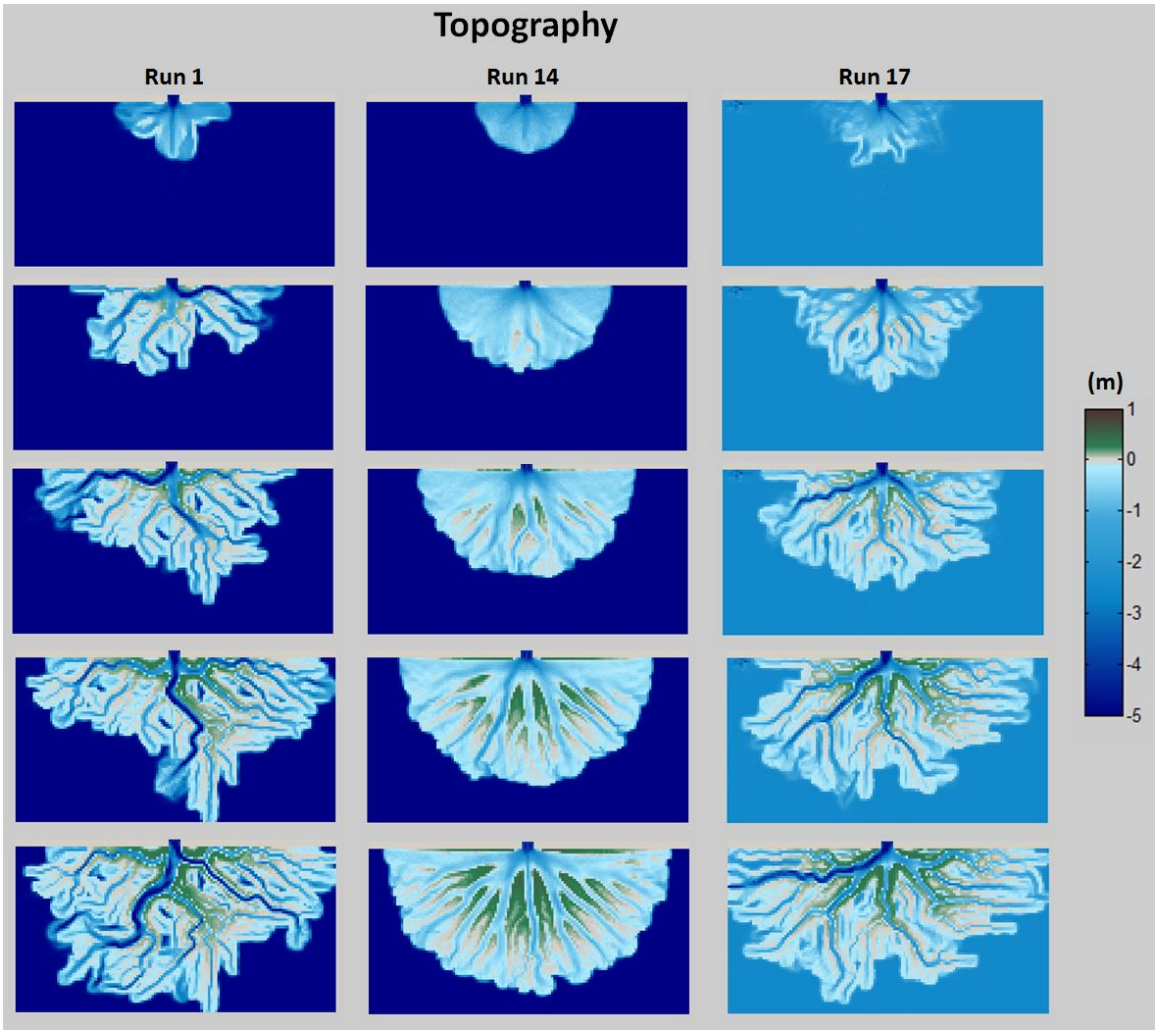

Figure 21: Temporal changes in topography for three delta runs.

To corroborate the visual comparisons, Figure 22 shows shoreline roughness values for the last time step in the runs. Taking the means of the deltas run at standard depth, the relative shoreline roughness decreases with increasing sand fraction, a trend

which confirms visual interpretation of the preceding maps. Since a perfect semicircle would yield a roughness value of $\sqrt{2\pi}$, this value is treated as an asymptote and a decaying logarithmic curve was fit to the data. Varying basin depth was also plotted, with the roughness increasing with increasing depth, although the mean roughness for the deep basin is not significantly greater than the mean for the standard-depth basin.

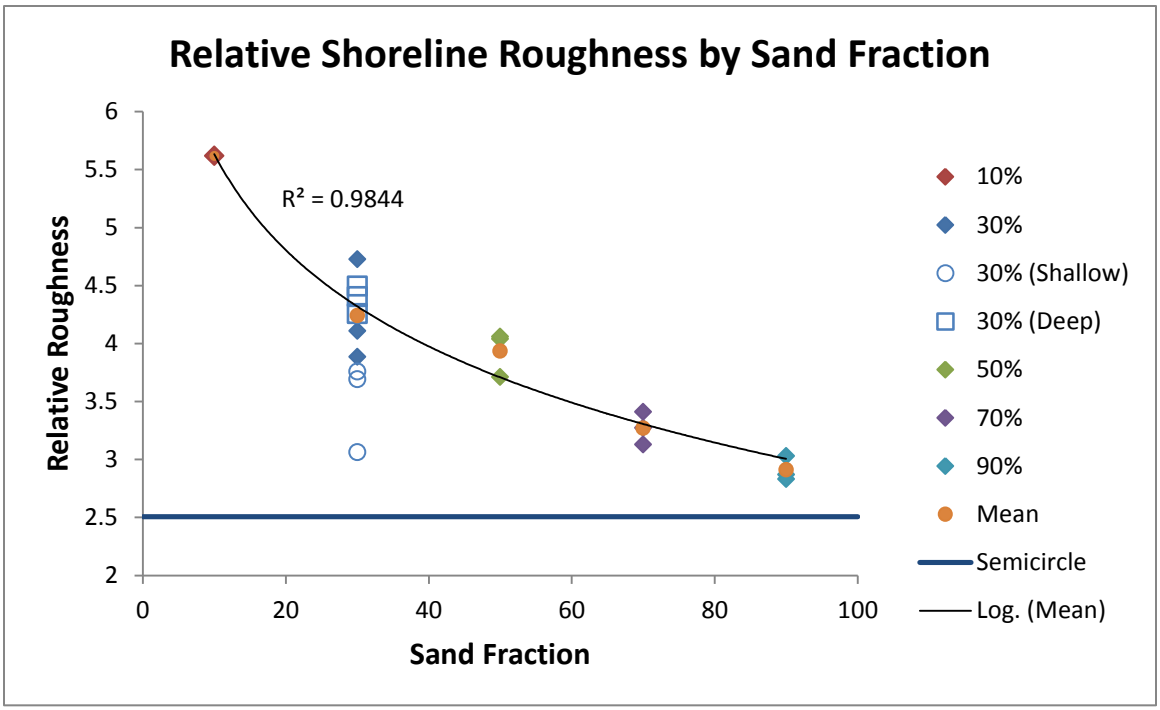

Figure 22: Relative shoreline roughness (equation 2) follows a decaying logarithmic pattern as the area becomes more like a semicircle.

METRIC COMPARISON

Delta Growth Metrics

Figure 23 shows the growth metrics for the *DeltaRCM* runs with varying sand fraction and basin depth. Figure 24 overlays two of these datasets (runs 1 and 10) on data compiled by Wolinsky et al. (2010).

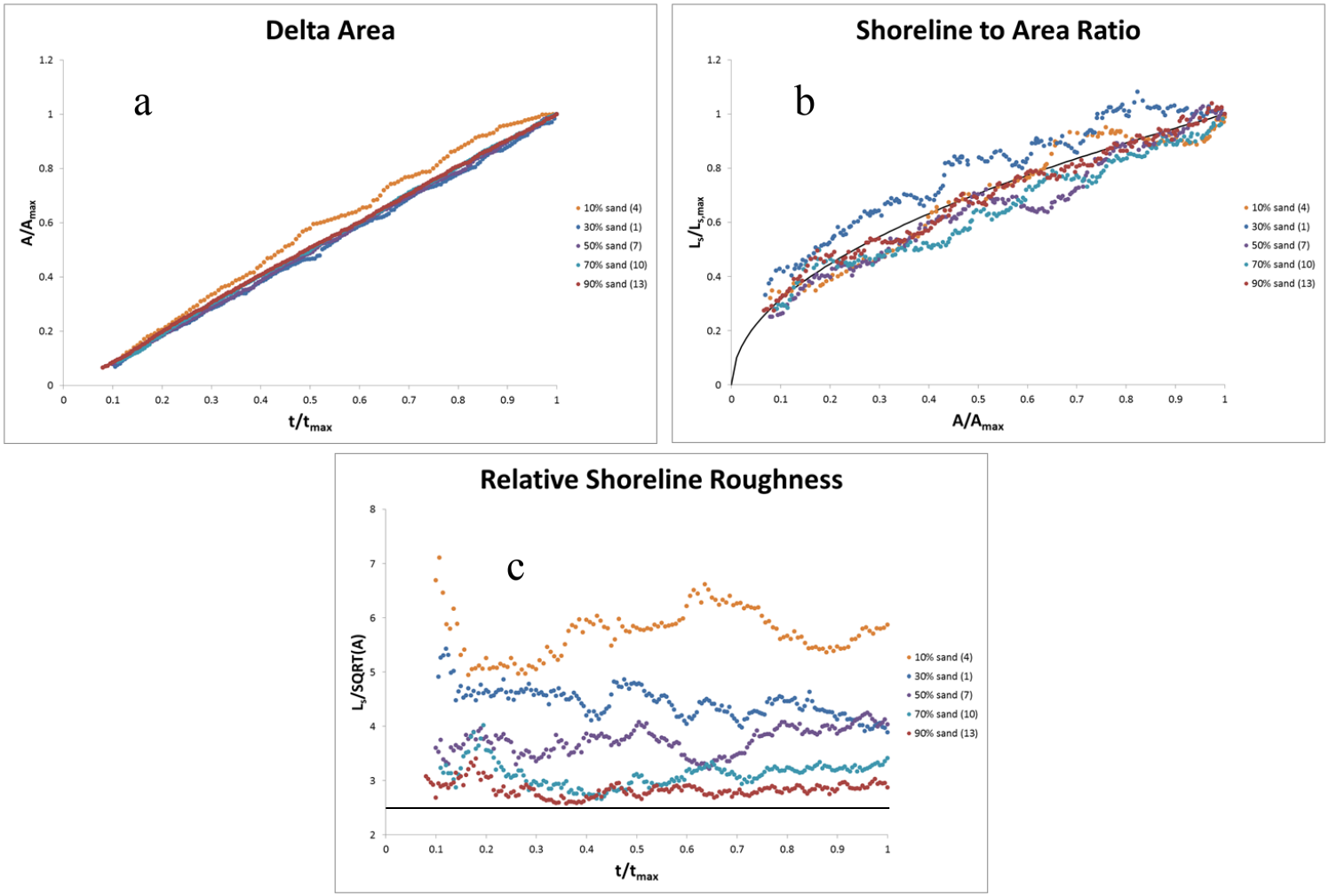

Figure 23: Delta growth metrics for varying sand fraction.

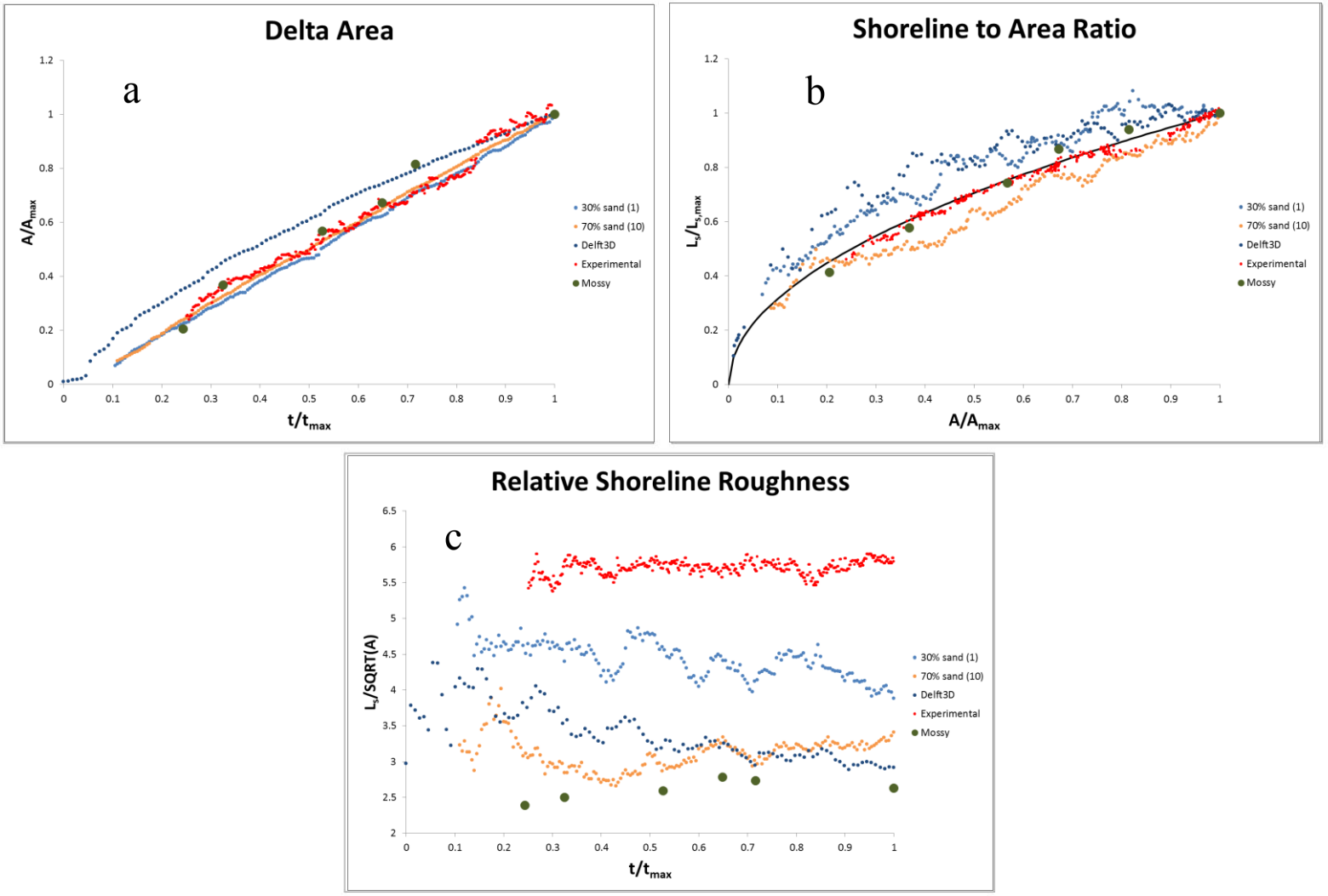

Figure 24: Delta growth metrics for two *DeltaRCM* runs, compared against data from Wolinsky et al. (2010).

Figure 23a shows that each *DeltaRCM* run grows at a constant rate for the entire run, which is reasonable since neither subsidence nor changes in influent characteristics change during the runs. The run with 10% sand fraction seems different because part of the delta left the bounds of the domain fairly early; the growth that occurred there was not captured, and thus the rate appears to slow down over time. The data presented are already truncated to a degree. The degree of roughening or smoothening over time is depicted in Figure 23b. When the data are above the square root curve (the black solid line), the delta is becoming more fractal, while data below the curve indicates the shoreline is becoming smoother. The data representing the lower sand fraction are on the fractal side of the curve here, while the higher sand fractions are on the smoothening side. This seems to contradict what Figure 21 suggests, that the structure of the deltas remain constant through time, though more runs would be necessary for making a conclusive decision. The data in Figure 23c are not surprising, though confirms that the trend observed in Figure 22 remains relatively constant through time.

Figure 24a shows runs 1 and 10 when compared against the data gathered by Wolinsky et al. (2010). Both *DeltaRCM* runs match well with Mossy Delta and the experimental delta. The Delft3D run included subsidence, so the land growth rate decreased over time. The shoreline-to-area ratio (Figure 24b) for the Mossy Delta and the experimental delta remain remarkably close to the square root curve, while both *DeltaRCM* and Delft3D deviate nontrivially, indicating that the degree to which the shoreline is fractal changes with delta growth. Finally, the relative shoreline roughness of the *DeltaRCM* runs fits comfortably between the values for the experimental and Mossy Delta.

Channel Overlap

The channel overlap as observed by Wickert et al. (2013) decayed very quickly for most of the experiments they analyzed, including the alluvial fan delta at a constant base level (Figure 25). The light gray represents fifty individual runs, while the darker grey is the average of those runs. The black line is a logarithmic fit.

DeltaRCM's deltas also have a decay of channel overlap, though not to the same value (Figure 26). Each dataset is the resultant mean of runs with identical input parameters. The runs with 50% sand had the least amount of channel overlap at the end,

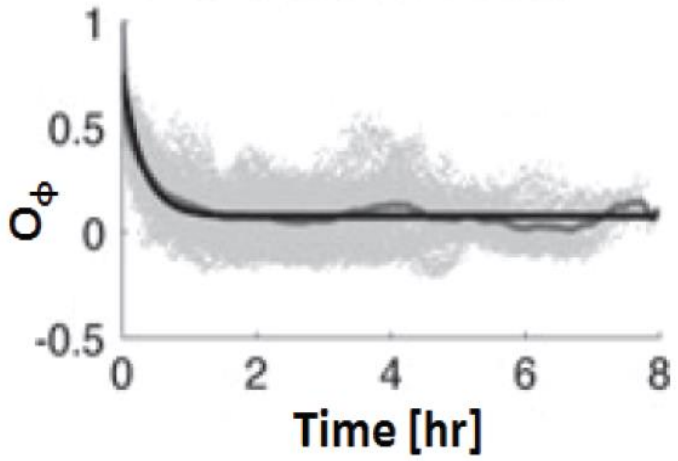

Figure 25: Channel overlap for XES02: base level constant, as performed by Kim et al. (2006) [Wickert et al., 2013].

with a value of about 0.12. 0.32 was the greatest final value, composed of those runs with 70% sand as the input. While it may not be statistically significant, these values suggest that *DeltaRCM* has a longer memory of channels than the experimental setup does.

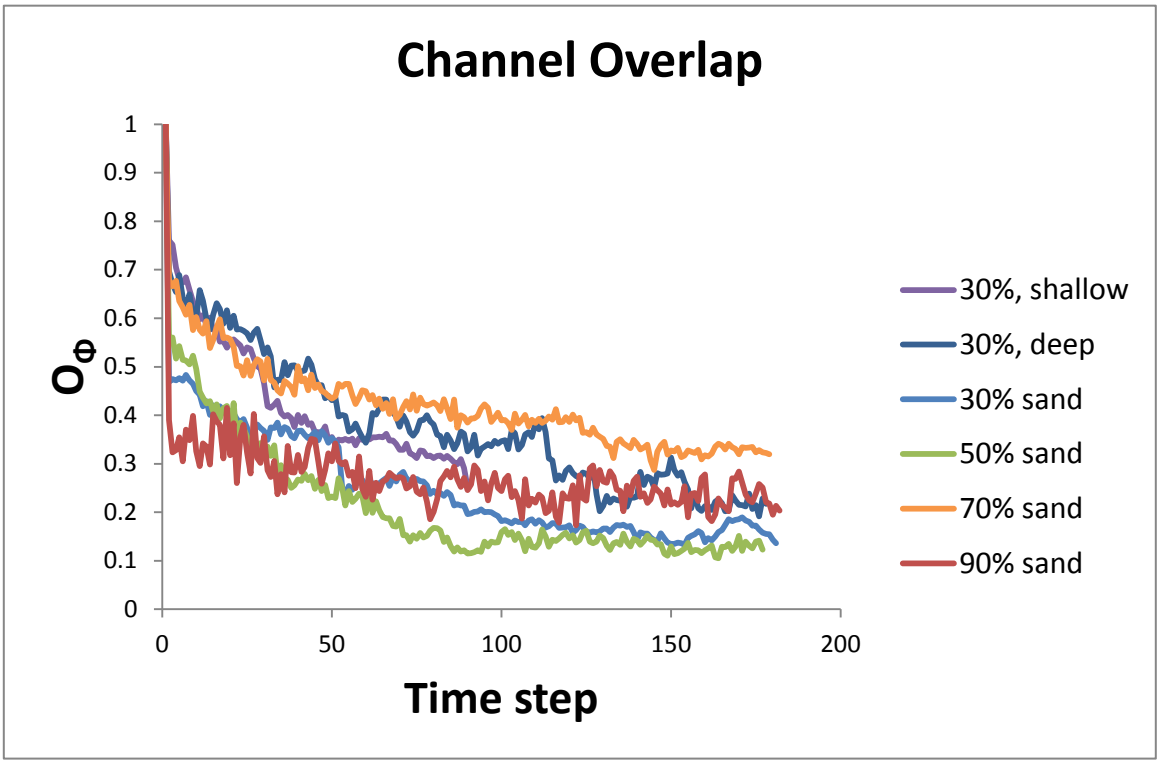

Figure 26: Averaged channel overlap for several *DeltaRCM* runs (deep data are truncated).

Avulsion Behavior

The temporal change of wetted fraction for the experiment performed by Reitz and Jerolmack (2012) is indicative of when and to what extent channel avulsions take place (Figure 27). The wetted fractions for the numerical runs (Figure 28) give a varying degree of avulsion evidence. For the low sand percentages (10% and 30%), crests and troughs are obvious in the wetted fraction, and visual analysis of the flow paths confirms that avulsions take place after local maxima. However, the relationship between the graphical features and the morphodynamic activities of the delta is not one-to-one. There are some falling segments that are not associated with a noticeable avulsion and some avulsions that do not seem to make their mark in the wetted fraction.

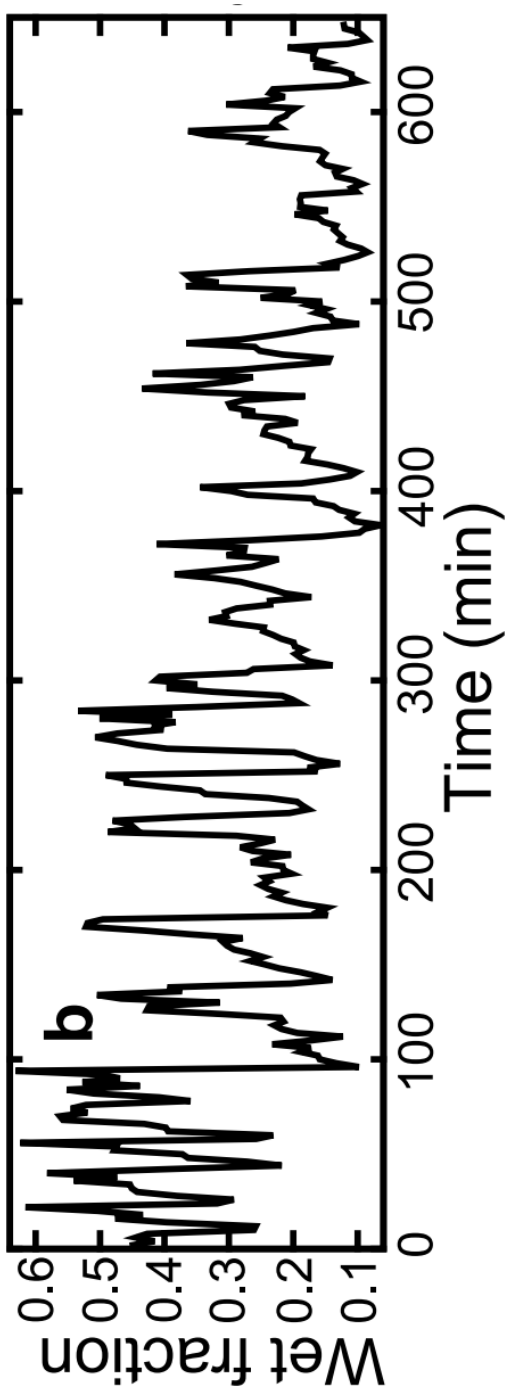

Figure 27: Wetted fraction for experimental delta by Reitz and Jerolmack (2012).

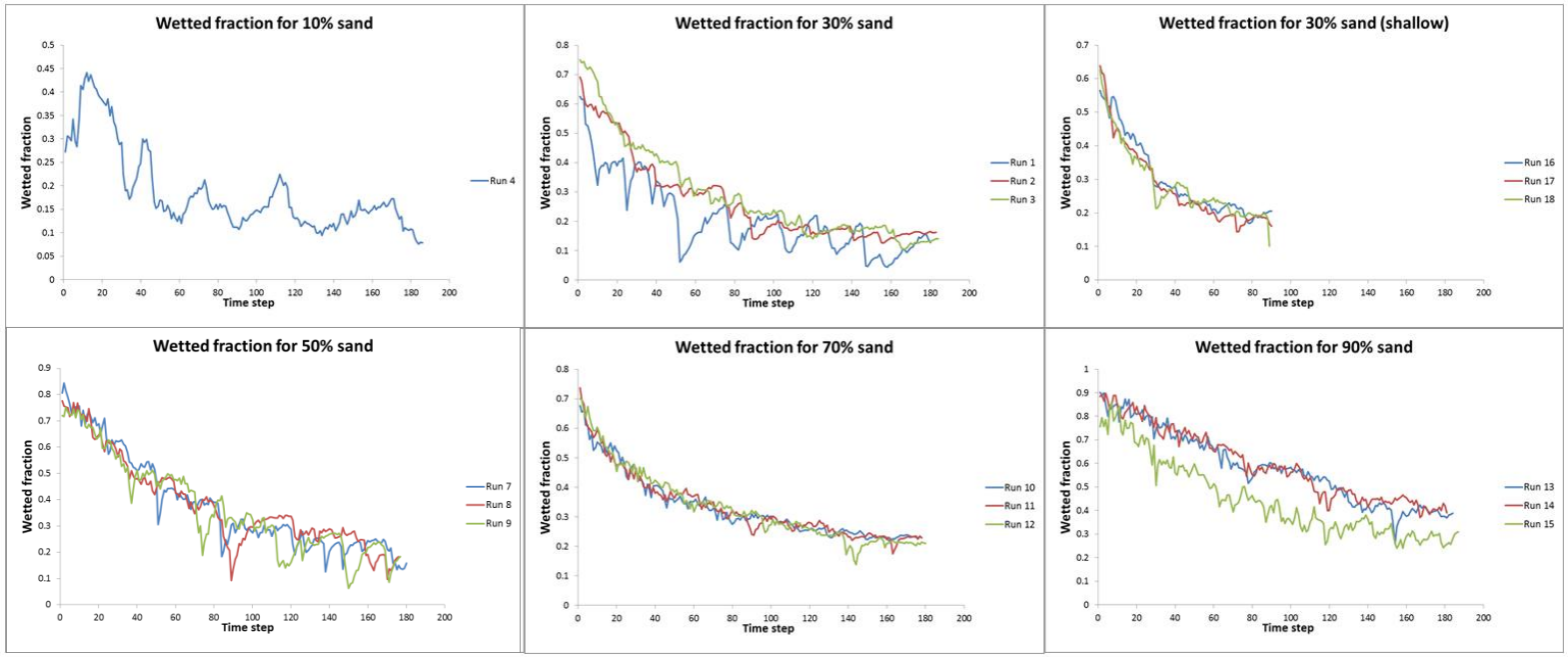

Figure 28: Wetted fraction through time for *DeltaRCM* runs.

Some of the ambiguity is reduced when the wetted fraction residual is obtained by subtracting the logarithmic trend from the data. The major drops in wetted fraction coincide with clear avulsive behavior, indicated by orange columns in Figure 29. However, there are still some instances, especially nearer the end of the run, in which the connection between channel avulsions and wetted fraction is not apparent.

Rough avulsion timescale estimates can still be made by looking at the distance between crests on the wetted fraction plot. Based on Figure 28, as well as confirmation through flow path analysis, significant avulsions occur on the order of 30 to 40 time steps for runs with 10% sand, or 25 to 32 years. This rate decreases slightly as sand fraction increases, until avulsions are unnoticeable (sandy deltas can be thought of as avulsing very frequently with very little magnitude, resulting in an even displacement of water and sediment). Decreasing the basin depth also decreases the avulsion time scale, which is reasonable since shallower water means the deltaic surface will aggrade toward the water surface faster to impede transport in the original direction.

Sedimentograph

The sedimentographs for the *DeltaRCM* runs are shown in the following figures, with each plot representing an average of runs with identical input parameters. Figure 30 portrays how the sedimentograph changes with varying sand fraction and Figure 31 with varying basin depth. Both of these figures give data for the final time step. For the varying sediment input, proximal deposits have high sand fractions, with a clear trend of fining towards the input fraction as the cross-sections move distally. For varying basin depth, trends are less clear, though it appears that deeper basins have lower sand fractions near the apex. Figure 32 shows how the deltas change through time: minor coarsening through time occurs throughout the delta, apart from the fining of sandy mouth bars.

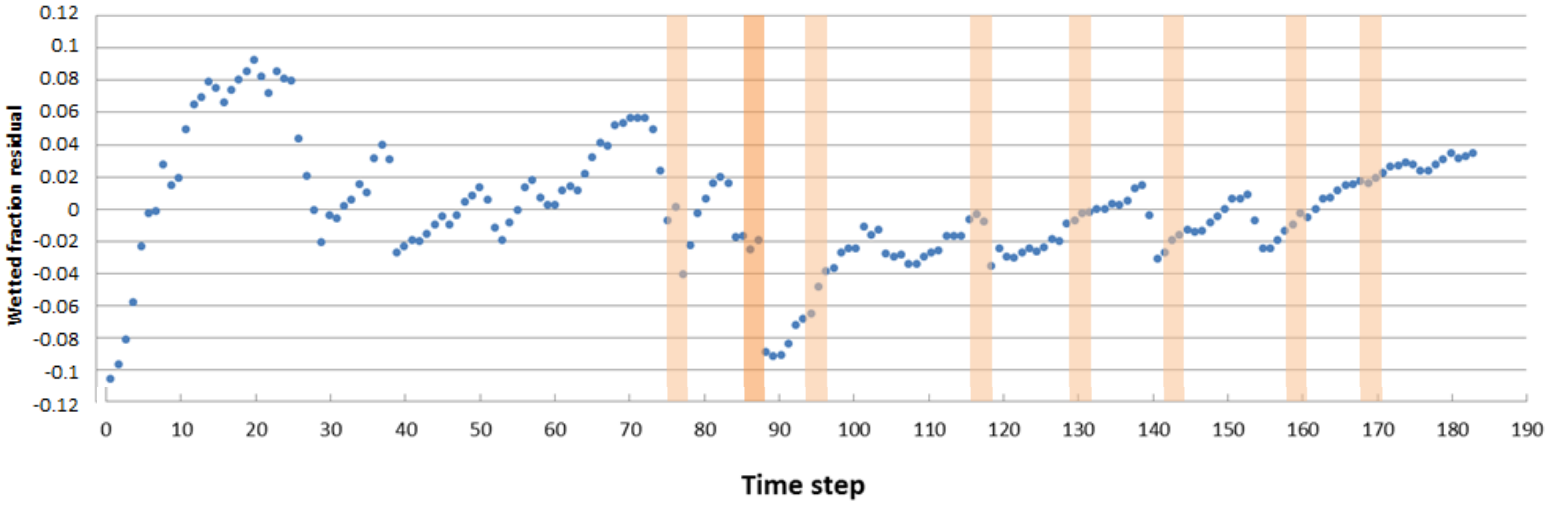

Figure 29: Wetted fraction residual for a standard-depth delta run. Orange bars refer to avulsions that could be seen in the flow path changes at those times. The dark orange bar represents a very large avulsion.

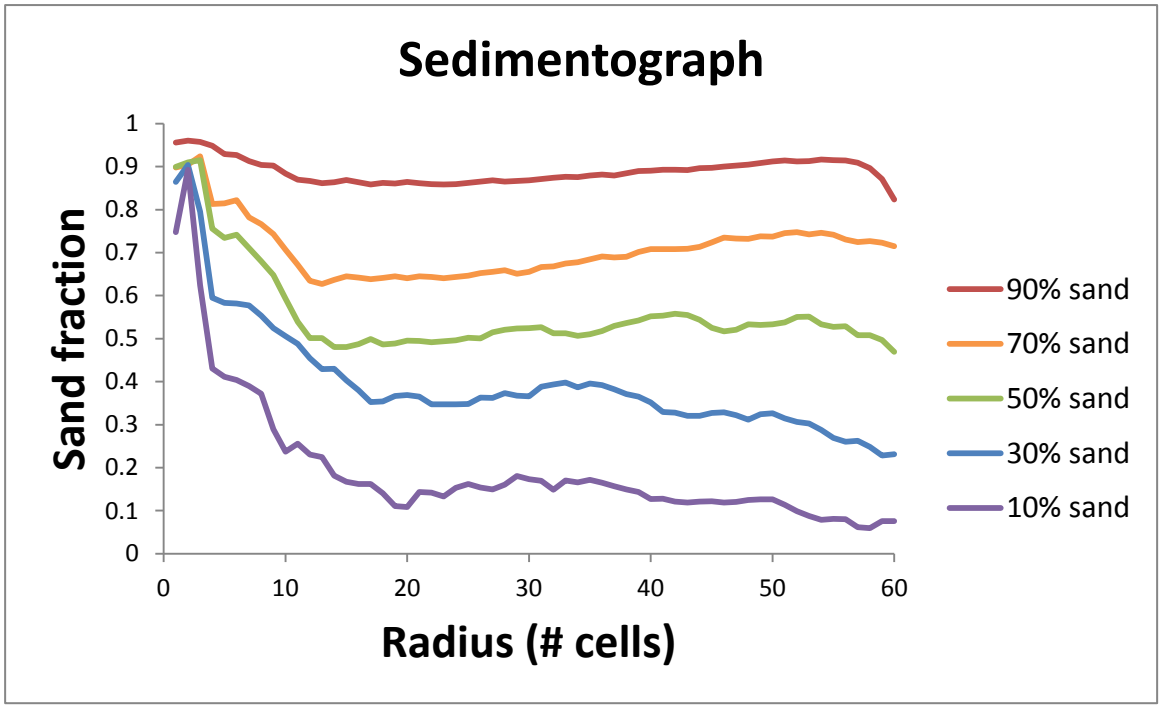

Figure 30: Averaged sedimentograph for varying sand fraction.

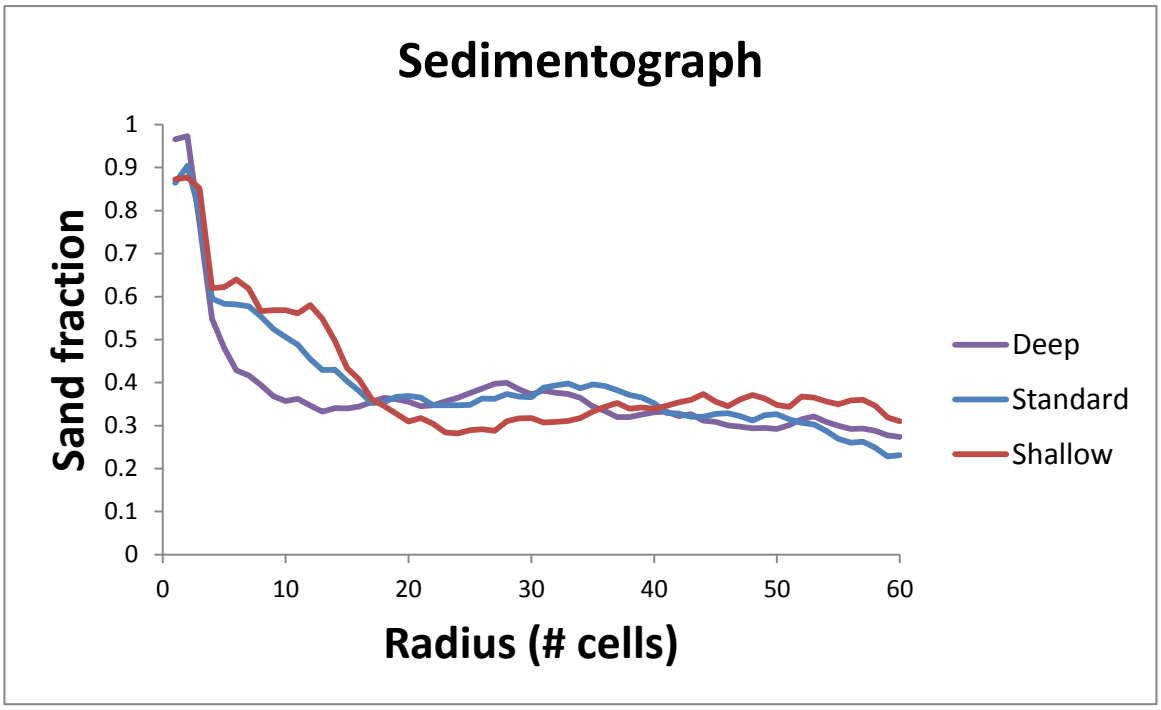

Figure 31: Averaged sedimentograph for varying basin depth.

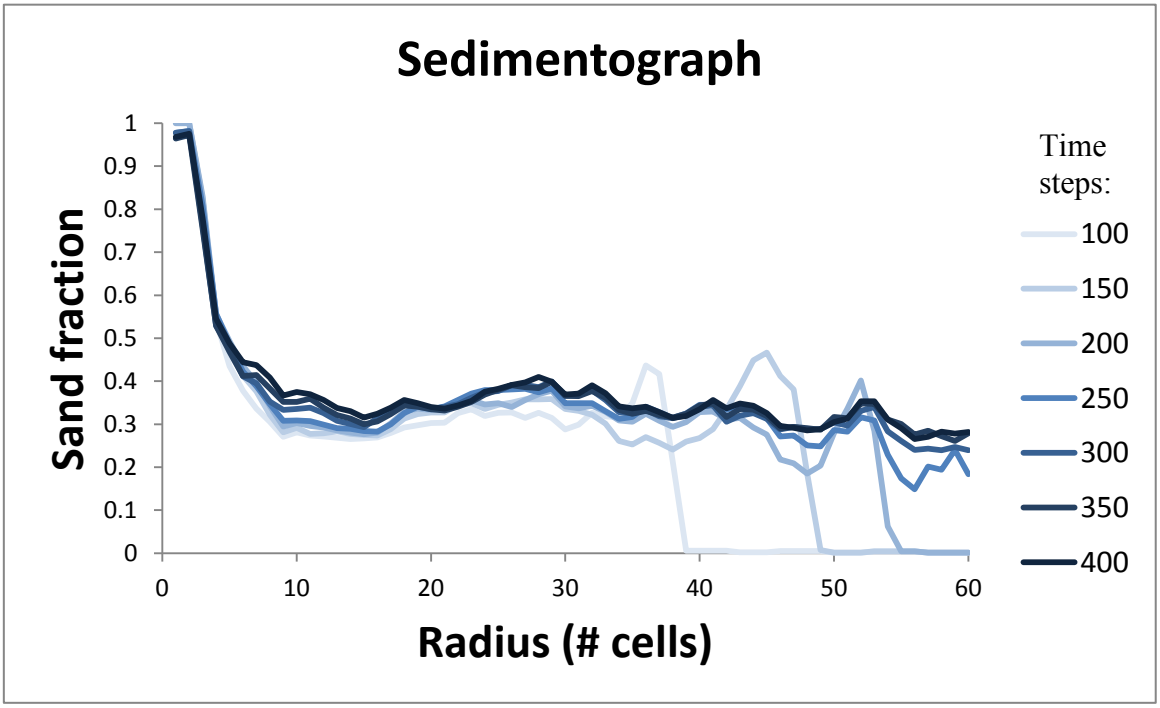

Figure 32: Sedimentograph through time for a deep-basin (run 19).

Chapter 5: Discussion

DeltaRCM performs well in creating deltaic structures based on internal consistency and morphodynamic metrics. Internal consistency is displayed very strongly in topography, delta age, and relative shoreline roughness. Patterns through time and across runs of varying parameters are regular, understandable, and consistent with reality. For example, as sand fraction increases, deltaic growth transitions from levee formation to island formation, a dynamic observed in nature (compare Figure 2 with the lower right corner of Figure 3). More work in the forms of additional runs or further statistical testing (e.g. delta age histograms) could be performed to corroborate internal consistency, though the existing results strongly support that *DeltaRCM* succeeds in this matter.

Internal consistency, however, is necessary but not sufficient for validating a numerical model. Satisfactory comparison to reality remains the more difficult piece in achieving a realistic model. Using the delta growth metrics introduced by Wolinsky et al. (2010), *DeltaRCM* compares remarkably well to experimental, field-scale, and numerical deltas. The normalized area through time remained highly linear as in the real systems, and the relative shoreline roughness for *DeltaRCM* fits between the bounds created by the real systems. While the shoreline-to-area ratio departs slightly from the square root curve that the real systems adhere to (indicating roughening over time), *DeltaRCM* demonstrates the trend at least as well as Delft3D. Especially if additional real systems are studied for these values, the shoreline-to-area ratio and relative shoreline roughness are solid metrics with which numerical models can be validated.

The performance when measured by the channel overlap is less conclusive. *DeltaRCM* produces deltas with consistently greater memory stored in the channel network than is exhibited by the experiments run by Kim et al. (2006), regardless of input

parameters. What this means as it pertains to the physics of *DeltaRCM* is unclear, and more work must be done to determine what significance, if any, this departure from the experimental systems entails. Validation of *DeltaRCM* and other morphodynamic numerical models would benefit from more experiments that analyze channel overlap and migration. Regardless, the general decay of overlap is encouraging.

As it stands, avulsion behavior has the weakest corroborating evidence for *DeltaRCM*'s accuracy. While the general trend of growth and rapid decay of the wetted fraction is contained in low-sand fraction runs, and larger avulsions are generally evident, there is no one-to-one relationship between drops in wetted fraction and avulsive behavior. The wetted fraction residual yields better but not definitive results. Supporting the idea that wetted fraction residuals are not completely reliable for avulsion prediction, runs with 70% or 90% sand, which grow without any noticeable avulsive activity, contain wetted fraction residuals that seem to indicate avulsions. Other metrics like channel density or shoreline-to-area ratio perform more poorly when used to predict avulsions. Automatic extraction of avulsions from a series of channel maps could prove useful in determining what metrics best predict avulsions, as visual inspection is time-consuming and error-prone. Finally, general trends for avulsion timescale are reasonable, though more runs should be performed to confirm these trends.

The sedimentograph, though it cannot be compared to real systems without extensive coring, is invaluable as it describes a delta's subsurface. The results obtained with the sedimentograph are generally unsurprising, though some important aspects of deltaic growth are demonstrated. The sedimentograph with varying depth explains that basin depth has little effect on the distances at which sand and mud are deposited, except at the apex, where a sudden change in depth has a great effect on where the sediment resides in the water column. Examining the data through time shows where sand and

mud collect as a delta grows and highlights sandy mouth bars at the shoreline. Better comparisons between deltas of different depths could be obtained by ensuring the runs contain the same total sediment volume.

Establishing a robust set of metrics would be very useful to the validation of models like *DeltaRCM*. The more that morphodynamic metrics are used to test models, the simpler and more vigorous future validation will be, as more data become available for comparison. The delta growth metrics, channel migration, and sedimentograph are great tools to be included in this "metric suite". Additional metrics that should be studied and tested for *DeltaRCM* are island statistics (i.e. size, shape) and compensation index, which would showcase the subsurface with a greater scope than the one-dimensional sedimentograph.

Chapter 6: Conclusions and Future Work

The primary goals of this work was to examine how well *DeltaRCM* works as a predictive model for deltaic growth and dynamics, particularly by looking at internal consistency and morphodynamic metrics as compared to real deltaic systems. *DeltaRCM* resolves deltaic growth very well when considering internal consistency, evincing both similarity and stochasticity between identical runs. When analyzing morphodynamic metrics, *DeltaRCM* excels for some, such as planform delta growth and relative shoreline roughness. For others, like channel overlap or avulsion timescale, the comparisons to experimental systems yield results that match well in terms of general trends but differ at closer inspection. Because existing metrics (both those examined here and otherwise) largely ignored the links between surface and subsurface, the sedimentograph was developed to describe and quantify behavior hidden from surface maps. Sedimentograph results are logical and coherent, which also bolster *DeltaRCM*'s credibility as a predictive tool.

Besides the establishment of additional metrics discussed at the end of the previous chapter, future work includes examining how localized and general subsidence affects delta growth and how a varying hydrograph or sediment inflow impacts the resulting delta. Investigating tidal cycles and vegetation are other long-term plans for *DeltaRCM*.

References

Campbell, W. G. 1990. Form and Style in Thesis Writing, a Manual of Style. Chicago: The University of Chicago Press.

Cahoon, D. R., D. H. White, and J. C. Lynch. 2011. Sediment infilling and wetland formation dynamics in an active crevasse splay of the Mississippi River delta. Geomorphology 131(3-4):57-68.

Caldwell, R. L., and D. A. Edmonds (2014), The effects of sediment properties on deltaic processes and morphologies: A numerical modeling study, J. Geophys. Res. Earth Surf., 119, 961–982.

Edmonds, D. A., C. Paola, D. C. J. D. Hoyal, and B. A. Sheets (2011), Quantitative metrics that describe river deltas and their channel networks, J. Geophys. Res., 116, F04022.

Edmonds, D. A., and R. L. Slingerland (2007), Mechanics of river mouth bar formation: Implications for the morphodynamics of delta distributary networks, J. Geophys. Res., 112, F02034.

Edmonds, D. A., C. Paola, D. C. J. D. Hoyal, and B. A. Sheets (2011), Quantitative metrics that describe river deltas and their channel networks, J. Geophys. Res., 116, F04022.

Ericson, J. P., C. J. Vorosmarty, S. L. Dingman, L. G. Ward and M. Meybeck (2006) Effective Sea Level Rise and Deltas: Causes of Change and Human Dimension Implication. Global and Planetary Change, 50, 63-82.

Kim, W., C. Paola, V. R. Voller, and J. B. Swenson (2006a), Experimental measurement of the relative importance of controls on shoreline migration, J. Sediment. Res., 76(2), 270–283.

Kim, W., D. Mohrig, R. Twilley, C. Paola, and G. Parker (2009), Is It Feasible to Build New Land in the Mississippi River Delta?, Eos Trans. AGU, 90(42), 373–374.

Lesser, G., J. Roelvink, J. van Kester, and G. Stelling (2004), Development and validation of a three-dimensional morphological model, Coastal Engineering, 51 (89), 883 – 915.

Liang, M., V. R. Voller, and C. Paola (2015a), A reduced-complexity model for river delta formation – Part 1: Modeling deltas with channel dynamics, Earth Surf. Dynam., 3, 67-86.

Liang, M., N. Geleynse, D. A. Edmonds, and P. Passalacqua (2015b), A reduced-complexity model for river delta formation – Part 2: Assessment of the flow routing scheme, Earth Surf. Dynam., 3, 87-104.

Liang, M., C. Van Dyk, and P. Passalacqua (2015c), Quantifying the patterns and dynamics of distributary channel networks in river deltas - assessment and application of a reduced-complexity model, in preparation for submission to Journal of Geophysical Research - Earth Surface.

Parker, G., T. Muto, Y. Akamatsu, W. E. Dietrich and J. W. Lauer (2008), Unravelling the conundrum of river response to rising sea-level from laboratory to field. Part I: Laboratory experiments. Sedimentology, 55: 1643–1655.

Passalacqua, P., S. Lanzoni, C. Paola, and A. Rinaldo (2013), Geomorphic signatures of deltaic processes and vegetation: The Ganges-Brahmaputra-Jamuna case study, J. Geophys. Res. Earth Surf., 118, 1838–1849.

Qu, F., J. Yu, S. Du, Y. Li, X. Lv, K. Ning, H. Wu, and L. Meng (2014), Influences of anthropogenic cultivation on C, N and P stoichiometry of reed-dominated coastal wetlands in the Yellow River Delta, Geoderma, 235-236, 227-232.

Rabalais, N., R. Turner, D. Justic, Q. Dortch, W. W. Jr., and B. S. Gupta (1996), Nutrient changes in the Mississippi River and system responses on the adjacent continental shelf, Estuaries, 19 (2B), 386–407.

Reitz, M. D., and D. J. Jerolmack (2012), Experimental alluvial fan evolution: Channel dynamics, slope controls, and shoreline growth, J. Geophys. Res., 117, F02021.

Kalyan, R. (2014), Changing river courses in the western part of the Ganga-Brahmaputra delta, Geomorph., 227, 87-100.

Seybold, H., J. S. Andrade Jr., and H. J. Herrmann: Modeling river delta formation, P. Natl. Acad. Sci. USA, 104, 16804–16809, 2007.

Shaw, J. B., D. Mohrig, and S. K. Whitman: The morphology and evolution of channels on the Wax Lake Delta, Louisiana, USA, J. Geophys. Res.-Earth, 118, 1–23, 2013.

Sun, T., C. Paola, G. Parker, and P. Meakin: Fluvial fan deltas: linking channel processes with large-scale morphodynamics, Water Resour. Res., 38, 26-1–26-10, 2002.

Syvitski, J., and Y. Saito (2007), Morphodynamics of deltas under the influence of humans, Global Planet. Change, 47, 261-282.

USGS Fact Sheet 2005-3101 (2005), Depicting Coastal Louisiana Land Loss, http://www.nwrc.usgs.gov/factshts/2005-3101/2005-3101.htm.

Wickert A. D., J. M. Martin, M. Tal, W. Kim, B. Sheets, and C. Paola (2013), River channel lateral mobility: metrics, time scales, and controls, J. Geophys. Res. Earth Surf., 118, 396–412.

Wolinsky, M. A., D. A. Edmonds, J. Martin, and C. Paola (2010), Delta allometry: Growth laws for river deltas, Geophys. Res. Lett., 37, L21403.